DEPARTMENT OF THE AIR FORCE

HEADQUARTES, 603D REGIONAL SUPPORT GROUP (USAFE)

European Office of Aerospace Research and Development

(EOARD)

Contract No. SPC 01-4057, Order number F61775-01-WE057

Awarded 10 July 2001

Final Report

Summarizing all progress on the tasks outlined in the proposal

Contract title: **Investigation of chemical generation of atomic Iodine for COIL, and testing of the supersonic COIL using diode probe diagnostics**

Investigators: **Otomar Špalek, Vít Jirásek, Miroslav Censký, Jarmila Kodymová**

Contractor: **Jarmila Kodymová**
Department of Gas Lasers
Institute of Physics
Academy of Sciences of the Czech Republic
Na Slovance 2
182 21 Prague 8
Czech Republic

Phone : 420-2-66052699
Fax: 420-2-86890527
E-mail: kodym@fzu.cz

Date: **10 July, 2002**

REPORT DOCUMENTATION PAGE

Form Approved OMB No. 0704-0188

Public reporting burden for this collection of information is estimated to average 1 hour per response, including the time for reviewing instructions, searching existing data sources, gathering and maintaining the data needed, and completing and reviewing the collection of information. Send comments regarding this burden estimate or any other aspect of this collection of information, including suggestions for reducing the burden, to Department of Defense, Washington Headquarters Services, Directorate for Information Operations and Reports (0704-0188), 1215 Jefferson Davis Highway, Suite 1204, Arlington, VA 22202-4302. Respondents should be aware that notwithstanding any other provision of law, no person shall be subject to any penalty for failing to comply with a collection of information if it does not display a currently valid OMB control number.
PLEASE DO NOT RETURN YOUR FORM TO THE ABOVE ADDRESS.

1. REPORT DATE *(DD-MM-YYYY)*	2. REPORT TYPE	3. DATES COVERED *(From – To)*
24-07-2002	Final Report	10 July 2001 - 21-Aug-02

4. TITLE AND SUBTITLE

Investigation Of Chemical Generation Of Atomic Iodine For COIL And Testing Of The Supersonic COIL Using Diode Probe Diagnostics

5a. CONTRACT NUMBER
F61775-01-WE057

5b. GRANT NUMBER

5c. PROGRAM ELEMENT NUMBER

6. AUTHOR(S)

Dr. Jarmila Kodymova

5d. PROJECT NUMBER

5d. TASK NUMBER

5e. WORK UNIT NUMBER

7. PERFORMING ORGANIZATION NAME(S) AND ADDRESS(ES)

Institute of Physics Academy of Sciences
Na Slovance 2
Prague 8 182 21
Czech Republic

8. PERFORMING ORGANIZATION REPORT NUMBER

N/A

9. SPONSORING/MONITORING AGENCY NAME(S) AND ADDRESS(ES)

EOARD
PSC 802 BOX 14
FPO 09499-0014

10. SPONSOR/MONITOR'S ACRONYM(S)

11. SPONSOR/MONITOR'S REPORT NUMBER(S)
SPC 01-4057

12. DISTRIBUTION/AVAILABILITY STATEMENT

Approved for public release; distribution is unlimited.

13. SUPPLEMENTARY NOTES

14. ABSTRACT

This report results from a contract tasking Institute of Physics Academy of Sciences as follows: The contractor will investigate the previously developed supersonic COIL driven by a jet singlet oxygen generator. Its operation will be explored using a tunable diode laser. They will also investigate the chemical generation of atomic iodine for a COIL using alternative chemical processes.

15. SUBJECT TERMS

EOARD, Laser spectroscopy, Molecular Chemistry, Chemical oxygen iodine lasers

16. SECURITY CLASSIFICATION OF:			17. LIMITATION OF ABSTRACT	18, NUMBER OF PAGES	19a. NAME OF RESPONSIBLE PERSON
a. REPORT	b. ABSTRACT	c. THIS PAGE			Alexander J. Glass, Ph. D.
UNCLAS	UNCLAS	UNCLAS	UL	65	19b. TELEPHONE NUMBER *(Include area code)* +44 (0)20 7514 4953

STATEMENT

(1) The Contractor, Institute of Physics of the Academy of Sciences, hereby declares that, to the best of its knowledge and believes, the technical data delivered herewith under Contract No. F61775-01-WE057 is complete, accurate, and complies with all requirements of the contract.

(2) I certify that there were no subject inventions to declare as defined in FAR 52.227-13, during the performance of the Contract No. F61775-01-WE057.

Name and Title of Contractor: Dr. Jarmila Kodymová

Name and Title of Authorized Official: Ing. Karel Jungwirth, DrSc.
Director of Institute of Physics

Date: 10 July, 2002

Content

Approved proposal of the contract No. F61775-01-WE057 has concerned the tasks outlined in the Schedule (see the next page).

The solved tasks were slightly modified on account of achievements during the contract progress. Dr. Gordon Hager, the contract supervisor at the US AFRL/DE, and Dr. Alexander Glass, Program Manager, Lasers, Photonics, and Optical Materials, at the USAF EOARD approved this.

The tasks concerned:

1/ Testing the COIL operation with modified jet SOG

- **The aim**: to improve the jet SOG operation in regard to the BHP droplets disengagement, and so to achieve an increasing in the output power and chemical efficiency of the COIL device in our laboratory

2/ Testing the COIL by using Iodine Scan Diode Probe diagnostics

- **The aim**: to perform a mapping the spatial gain and temperature distribution across the gain region, and to find the optimum mixing conditions in the COIL

3/ Investigation of chemical generation of atomic iodine

a) via Cl atoms concerned

- Investigation of reaction kinetics on a small-scale device in nitrogen flow and singlet oxygen flow (gain measurements on $I(^2P_{1/2}) - I(^2P_{3/2})$ transition by using the diode laser probe diagnostics)
- Constructional modifications of our COIL device for investigation of atomic iodine generation in the COIL device (injection of reactants into the primary flow containing $O_2(^1\Delta_g)$)
- Investigation of atomic iodine generation in the modified COIL device
- Utilization of results of 1-D and 2-D modeling for interpretation of experimental results

b) via F atoms concerned

- 1-D modeling of atomic iodine generation in conditions similar to a COIL
- 1-D modeling of F_2/NO/HI mixture for a design of small-scale device for experimental investigation

Schedule for tasks solved in the framework of the contract

	2001						2002					
	7	8	9	10	11	12	1	2	3	4	5	6
Testing COIL with modified jet SOG												
Testing COIL with Diode laser diagnostics												
Atomic iodine generation via Cl atoms												
Design of small-scale device with jet SOG												
Fabrication and testing of device												
Investigation of gain on I atom transition												
Atomic iodine generation via F atoms												
Literature review, calculations for device design												
Design of small-scale device												
Fabrication of individual parts												
Installation												
Testing of individual parts of device												
First experiments with F and I generation												
1D or 2D model of I production via F and Cl atoms												
Reports to EOARD												

1. Testing the COIL operation with constructionally modified jet singlet oxygen generator (jet SOG)

The jet SOG with a vertical gas exit and with additional constructional modifications was employed at the COIL operation instead of previously used jet SOG with a side gas exit. It was aimed to enhance **a passive liquid (BHP) disengagement from gas exiting the generator**. It should help to solve a serious problem that generally comes along the jet SOGs operation, i.e., liquid (BHP) droplets escaping with a gas exiting the generator. These droplets are evaporated and form a solid layer on the walls of the gas channel and nozzle throat, diminishing so their cross section besides blocking the holes of iodine injector placed in the walls of the gas channel. Further, the BHP aerosol flies into the laser cavity where it can cause a light scattering on the solid BHP particles. The jet SOG with a side exit did not bring an effectual removing of this problem even if the BHP "directors" were installed into a space above the BHP injector and several modifications of the generator gas exit were tested (see Final Report of the previous contract F61775-00-WE032, submitted on 4 April 2001).

1.1. Constructional modifications of "vertical" jet SOG and tested effects

The jet SOG with vertical gas exit was schematically shown already in the Final Report of the previous contract, and in this report, it is in **Fig. 1**. A substantial decrease in liquid droplets entraining with gas was expected in this design by a larger cross-section of the gas stream crossing the last rows of liquid jets. To diminish a loss of singlet oxygen, two fillers were still inserted into a gas space in the upper part of generator.

Some constructional modifications and changes of generator parameters (e.g., an increase in the BHP jets velocity from 5.7 m/s up to 8.2 m/s), were tested and these results were summarized also in the Final Report of the previous contract. Further introduced modifications of this jet SOG and their testing during this contract are mentioned bellow.

First we tested the BHP injector without inserted stainless steel needles into injector holes. Then the needless of 1.2/0.9 mm and 20mm or 40 mm long were inserted into two rows of orifices around the exiting tubular gas channels. Finally, the needles of 1.2/0.9 mm and 18 mm long were inserted into all holes of the BHP injector (see **Fig. 1**). To prevent a preferential flow of gas (chlorine) through the middle gas channel between jets below the exiting tubes, and to reduce the volume of the generator, a 10 mm vertical plate was inserted into this channel (see **Fig. 1**). To increase the BHP droplets disengagement, the exiting tubes

in the upper part were bent to direct the exiting gas against the vertical wall where the droplets should be separated owing to a sudden change in gas flow direction (see **Fig. 1**).

A casual plugging the holes in the chlorine injector at the generator bottom (occurring at jetting without introducing the primary gas) was avoided by increasing a number of the holes (1 mm i.d.) in it from 12 to 34 mm.

1.2. Results of testing and conclusions from this investigation

- The BHP escaping into the exiting gas was decreased in operation of the jet SOG with vertical gas exit in comparison with the generator with side gas exit.
- The singlet oxygen yield measured in the optical cell placed in the gas channel downstream form the generator exit achieved similar values as in the generator with side exit (40 - 80 % at the generator pressure of 10 - 3.8 kPa, i.e. 75 – 28.5 torr).
- The BHP droplets disengagement from the exiting gas was most effective by inserting the needles into all holes of the BHP injector, and by a blocking the middle channel with the vertical plate simultaneously. Several experimental runs of COIL operation could be performed without observing a BHP settling on the channel walls with this jet SOG, which means that the BHP escaping with the outlet gas was substantially suppressed. A BHP droplets escaping worsened with increasing the BHP temperature, and during longer BHP recirculation (several minutes) due to its oversaturation with dissolved oxygen. This problem accompanies generally the operation of all jet SOGs that employ the BHP recirculation.
- The above-mentioned improvement of the jet SOG operation had, unfortunately, no substantial effect on an increase in the laser power and so the chemical efficiency of our COIL device, even though reasonable high values of small signal gain were recorded (see chap. 2.2). There are at least two explanations of this fact: i) high inner cavity losses by a light scattering on solid BHP particles, and ii) bad quality of the resonator outcouplers used during these measurements. Unfortunately, neither the last modification of the jet SOG with the bent tubes for exiting gas nor the newly purchased resonator mirrors could be tested because of recent failure the vacuum pumping complex.
- It can be concluded that a passive disengagement of the BHP liquid from the gas flow by means of the appropriate generator modifications can be rather effectual but mostly during a short jet SOG operation only.

- Another ways of BHP disengagement, both passive and active, will be searched.
- New resonator mirrors will be tested to check again the chemical efficiency of our COIL device when the vacuum complex is repaired.

2. Testing the COIL by using the Iodine Scan diode probe laser diagnostics

The results of mapping a spatial gain distribution and temperature evaluation in the gain region of supersonic COIL device by using the Iodine Scan Diagnostics were presented in details in the interim Report 0001 of this contract submitted to the EOARD on 10th October 2001. Therefore, only main results and conclusions of this investigation are summarized in this Final Report.

2.1. Summary of experimental conditions

During all performed measurements, the primary gas flow was 40 mmol Cl_2 s^{-1} and 80 mmol He_{prim} s^{-1}. At this dilution ratio, the jet SOG operation was most stable, and the generator provided rather high $O_2(^1\Delta_g)$ yield (70–80 %) at generator pressure of 7.5 to 9.0 kPa (56 to 67 torr). The I_2 flow rate was varied between 1 to 2 mmol s^{-1}, and He_{sec} flow rate between 40 to 80 mmol s^{-1}. The plenum pressure was 3.4 to 4 kPa (25 to 30 torr), the cavity pressure was 300 to 390 Pa (2.2 to 2.8 torr).The gain length was 5 cm, and the plenum distance from the optical axis was 5.5 cm. The gain data were extracted from a two-passed probe beam configuration, and the probe beam emitter/detector unit and the mirror system for beam alignment were mounted on an assembly of motorized linear positioning equipment. This instrument allowed fast and precise movements either in horizontal direction (x axis) along the gas flow or vertical direction (y axis) perpendicular to the gas flow. A positional dependence of the gain was recorded at three horizontal levels: at the cavity center, 0.55 cm above and 0.55 cm below the center, respectively, and at three vertical planes, 4.1, 5.5, or 7 cm distant from the nozzle throat.

2.2. Results of investigation

The gain distribution along the vertical plane passing through the optical axis (i.e., 5.5 cm from the nozzle throat) is shown in **Fig. 2,** recorded at three different I_2 flow rates within 1.2 to 1.75 mmol s^{-1}, and 80 mmol He_{sec} s^{-1}. The highest gain of 0.9 %/cm was observed at 1.5

mmol I_2 s^{-1}. A parabolic shape of the gain distribution indicated that the gas flow velocity was inhomogeneous across the gain region. In both boundary layers along the walls, the gas velocity was slower resulting in remarkable quenching of I^*, and in an exhausting of $O_2(^1\Delta_g)$ still before the gas reached the gain region. Also I_2 molecules in an excess could be present in these layers (relative to its average concentration), which might cause an increase the $O_2(^1\Delta_g)$ consumption for I_2 dissociation. More intensive I* quenching by I_2 molecules could also occur. An observed "attenuation" of the probe signal in the boundary layers (0.5 to 1.5 mm thick) indicated prevailing atomic iodine in the ground state over the excited state in these layers. This interpretation was supported by determination of the gas temperature (calculated from these measurements), which was in these boundary layers much higher (350–600 K) than in the center of the gas channel (175–205 K). An inhomogeneous gas temperature across the gain region is obviously affected by more intensive exothermic processes per unit length in the flow direction. Due to a low velocity and insufficient gas cooling by isentropic gas expansion near the cavity walls, the temperature is substantial higher.

The gain and its distribution were strongly affected by the flow rate of secondary helium. It is demonstrated in **Figs. 3** and **4**. At the optimum I_2 flow rate of 1.5 mmol s^{-1}, the gain grows nearly linearly with He_{sec} flow from 40 to 80 mmol s^{-1}. A two peak-course of gain with the minimum in the cavity center (see **Fig. 5**) was observed at 40 mmol He_{sec} s^{-1}. An insufficient mixing of primary and secondary gases (a poor penetration) caused evidently lower gain values in the cavity center. In this case, the boundary layers are oversaturated with molecular and atomic iodine in the ground state, while there is a shortage of iodine in the cavity center. The effect of penetration of secondary flow into the primary flow was estimated by evaluation of the penetration factor for various flow conditions. **Fig. 6** illustrates that the best gain was recorded in the case when the penetration factor approached to unit, which was obtained at 80 mmol He_{sec} s^{-1} and 1.5 mmol I_2 s^{-1}.

Similar parabolic curves of gain distribution as in **Fig. 2** were recorded at a distance of 4.1 cm, i.e., 1.4 cm upstream from the cavity center. In these measurements, the gain increased monotonically with I_2 flow rate up to the highest value of 1.0 %/cm at 1.77 mmol I_2/s (see **Fig. 7**).

Fig. 8 shows the effect of I_2 flow rate on the gain measured in the cavity center but at different distances from the nozzle throat. Lower gain upstream the resonator axis measured at 1.2 mmol I_2 s^{-1} can be ascribed to a slower I_2 dissociation and so a lack of I^*. The reverse course at 1.75 mmol I_2 s^{-1} can be explained by the initial fast I_2 dissociation and following rapid I^* quenching by excessive I_2 molecules.

The small signal gain was also affected by operation parameters of the jet SOG. It was observed that even small decrease in the generator pressure from 8.3 kPa (62 torr) to 7.3 kPa (55 torr) resulted in increasing in the gain by 0.2–0.4 %/cm. By lowering the generator pressure, the $O_2(^1\Delta_g)$ yield increased, having a positive effect on the gain. On the other hand, a gradual lowering the pressure, resulting in a higher gas velocity in the jet SOG, increased the BHP droplets escaping from the generator into the cavity.

The gain mapping was performed also in the flow direction (by horizontal probe moving) in the cavity center at different distances from the nozzle throat. The dependences in **Fig. 9** recorded for three values of I_2 flow rate and constant He_{sec} flow rate of 40 mmol s^{-1} showed "waves", which revealed an existence of inhomogenities in the gain medium along the supersonic flow in the cavity due to a non-optimum penetration (40 mmol s^{-1} of He_{sec} only).

The gas temperature was evaluated from the recorded dependences of gain vs. frequency. The temperature of 175 to 205 K (± 15 K) was calculated for the cavity center. It was higher by ~15 K when He_{sec} was decreased from 80 mmol s^{-1} to 40 mmol s^{-1}. The I_2 flow rate did not affect substantially the gas temperature. It was also increased by ~ 25 K with increasing distance from the nozzle throat (from 4.1 to 7 cm). In the boundary layers, the gas temperature (evaluated from the recorded dependences of loss vs. frequency) was much higher, attaining 350 to 500 K (even 600 K).

2.3. Conclusions from this investigation

- The gain of nearly ~1%/cm was achieved in the center of cavity of our supersonic COIL under optimal mixing conditions (40 mmol Cl_2 s^{-1} + 80 mmol He_{prim} s^{-1}, and 1.5 mmol I_2 s^{-1} + 80 mmol He_{sec} s^{-1}).
- In comparison with the results on gain measurements reported from the AFRL[1], the gain in our COIL device was approximately 1.7 times higher than in the ReCOIL device, and 1.5 times higher than in the ROTOCOIL device. A dilution ratio of Cl_2:He_{total} was 1:4 in these devices, and pressures in the cavity was 2.38 torr in the ReCOIL, and 3.9 torr in the ROTOCOIL (2.2–2.8 torr in our COIL). The gain measured in the RADICL device was higher (1,2 %/cm) but also the ratio of He_{prim}/Cl_2 was substantially higher (5.3), and the cavity pressure as well (5.8 torr). It could be supposed that the gain would also increase in our COIL with increasing in the cavity pressure thanks to the fact that the jet SOG provides

higher $O_2(^1\Delta_g)$ yields (70 - 80 %) than roto-generators (60 %). These experiments are planned in future.

3. Chemical generation of atomic iodine for a COIL

3.1. Experimental investigation of atomic iodine generation via reaction Cl + HI

Description of this reaction system and its modeling was presented in details in the Final Report of the previous contract and in the interim Report 002 of this contract. In this report, the experimental procedure and the results are summarized, and currently solved tasks are outlined.

3.1.1. Investigation on a small-scale device with Iodine Scan Diagnostics beam parallel to gas flow

A detail description of the pilot small-scale device was presented in the interim Report 001 of this contract, and here is schematically shown in **Fig. 10**. The reactor was designed for investigation of the rate of atomic chlorine production followed by atomic iodine production under flow and pressure conditions that simulated these conditions in our COIL. The cross section of the reactor is shown in **Fig. 11** including the movable injectors inserted coaxially in the reactor bends for injection of individual reactants (ClO_2, NO, and HI). The pressure in the reactor was 1.5–4 kPa with gas velocity 130–160 m s^{-1}. The reactants entered the reactor at room temperature. The optical cell for atomic iodine detection by the Iodine Scan Diagnostics (ISD) (11 mm i.d., 45 mm of inner length) was close coupled to the reactor due to a short lifetime of iodine atoms in studied gas mixtures (0.2–1 ms). The gas flow through the cell was longitudinal because of the low flow rate of reactants and produced atomic iodine as well, and for a necessity to have a sufficient absorption length. In this ISD cell arrangement, however, only average concentrations of atomic iodine could be measured (not local concentrations). It was a certain initial drawback of this experimental arrangement. The gas velocity downstream from the reactor and through the ISD cell was 80–90 m/s. The atomic iodine flow rate was determined also indirectly from the measured concentration of I_2 molecules that were formed by recombination of iodine atoms. The I_2 concentration was measured at some distances from the reactor by VIS absorption photometry at 488 nm using the Argon ion laser.

The experimental investigation was first performed in an environment of nitrogen to prove this new method of atomic iodine generation in some non-reactive gas. The process was then studied in a flow of reactive singlet oxygen. In this case, the device was equipped with the jet SOG and diagnostics for $O_2(^1\Delta_g)$ detection.

During experiments in nitrogen flow, the primary gas flowing into the reactor consisted of 4-10 % ClO_2 in nitrogen, and a mixture of NO and nitrogen (10 % NO) was introduced through first or second injector or through both injectors simultaneously. A mixture of HI and N_2 (with 8-10% HI) was introduced in the most experiments through the 3rd injector. The flow rates of reactants were: up to 0.24 mmol ClO_2 s^{-1} in the primary flow, up to 0.6 mmol NO s^{-1}, and up to 0.5 mmol HI s^{-1}.

The production of atomic iodine in the flow of singlet oxygen was performed in the same reactor but the $O_2(^1\Delta_g)$ stream was introduced as the primary gas. The ClO_2+N_2 mixture was introduced through the 1st injector, the NO+N_2 mixture through the 2nd injector, and HI+N_2 mixture through the 3rd injector.

Further operation procedure and conditions including ClO_2 production, and study of I_2 production through other processes than via atomic iodine recombination were described in details in the interim Reports 0001 and 002 of this contract.

3.1.1.1. Results of atomic iodine generation in nitrogen environment and their discussion

First, atomic iodine generation was studied at different flow rates of reactants. An example of the effect of HI flow rate is shown in **Fig. 12**. It can be seen that the overall production of atomic iodine (detected by VIS photometry) was rather high and increased with increasing HI flow rate. The atomic iodine yield, however, declined from nearly 100% to 80% with increasing HI flow rate. The production rate calculated from the ISD method was significantly lower. This was caused by a drop in the atomic iodine concentration in the flow direction downstream of the reactor. This was confirmed by the results of our modeling studies calculated for the same experimental conditions that are shown in **Fig. 13**. The calculated curves demonstrate that the average flow rate of atomic iodine through the ISD cell is substantially lower than the overall rate of I formation, which is approximately equal to twice the value of the I_2 flow rate through the first I_2 detection cell. The flow rate of atomic iodine measured by the ISD increased with HI flow rate to some limit only (see **Fig. 12**). This can be explained by the higher rate of I atom formation and recombination at the higher HI flow rates. This results in a steeper concentration gradient of atomic iodine downstream of the HI

injection point, and a smaller fraction of the I flow rate being detected in the ISD cell compared to the overall production rate.

In the next experiments, the effect of the way in which NO was injected into the primary flow on atomic iodine production was studied. Nitrogen oxide was injected into the primary ClO_2 flow either through the first or the second injector, or both injectors simultaneously. The results are summarized in **Table 1**.

Tab. 1

Effect of the position of NO injection on atomic iodine production measured by ISD (n_I^{ISD}), and VIS photometry (n_I^{VIS}). Primary flow: 220 μmol ClO_2 s^{-1}+2 mmol N_2 s^{-1}, distance between injectors: d_{1-2}= 30 mm, d_{2-3}= 3.7 mm, and 3rd injector - ISD cell: d_{3-ISD} = 20 mm

n_{NO} (1st inj.), μmol /s	n_{NO} (2nd inj.), μmol /s	n_{HI} (3rd inj.), μmol /s	n_I^{ISD}, μmol /s	n_I^{VIS}, μmol /s
320	0	100	0	18
200	200	100	8	46
0	420	100	20	75

The lowest production of atomic iodine was measured when NO was introduced through the first injector only. This is because a high fraction of chlorine atoms was recombined upstream the HI injection. This was confirmed by the calculated decrease in Cl atom concentration (along the gas flow). **Fig. 14** shows that the calculated decrease in Cl atoms production with the distance. The Cl yield of 5% only was estimated at a distance of 33.7 mm between the NO and HI injectors. The measured yield of I atom formation (see **Table 1**) was higher than the above value, which may be explained by a limited gas mixing rate that extends the concentration profiles.

The rate of I atom formation was much higher when the NO was injected into the primary flow sequentially through the first and second injector. In this way, ClO radicals are formed mostly downstream of the first injector, and Cl atoms downstream of the second injector, which is illustrated in **Fig. 15**. It was further found experimentally that the rate of I production was not influenced by the distance between the NO injectors (within 8 to 21 mm). This can be explained by the relatively high stability of ClO radicals downstream of the first NO injector (see **Fig. 15**).

The highest yield of atomic iodine (see **Table 1**) was attained when all the NO was introduced through the second injector and HI was injected downstream (3.7 mm). This

distance between the injectors is close to the optimum corresponding to the calculated maximum concentration of Cl atoms (see **Fig. 14**).

In other experiments, the NO flow was split between two injectors. Effects of the variable distance between the two injectors are presented in **Table 2**.

Tab. 2

Effect of distance between injectors on atomic iodine flow rate, measured by ISD (n_I^{ISD}), and VIS photometry (n_I^{VIS}). Primary flow: 240 μmol ClO_2 s^{-1}, 1st injector: 220 μmol NO s^{-1}, 2nd injector: 220 μmol NO s^{-1}, 3rd injector: 100 μmol HI s^{-1}, total N_2 7.2 mmol s^{-1}

d_{1-2}, mm	d_{2-3}, mm	$d_{3\text{-cell }11}$, mm	n_I^{ISD}, μmol /s	n_I^{VIS}, μmol /s
9	23	20	0.5	15
19	13	20	3	35
37	3.7	20	6	54
37	3.7	10	10	55

These data show the positive effect of a shorter distance between the second NO injector and the HI injector on I atom production in spite of a simultaneously longer distance between the 1st and 2nd NO injector. This is due to a lower recombination loss rate of Cl atoms upstream of the HI injector. A higher concentration of I atoms in the ISD cell was measured with a shorter distance between the HI injector and the cell, even though the overall rate of I atom formation remained unchanged. This was caused by a lower loss of iodine atoms by recombination reactions upstream of the ISD cell.

The generation of iodine atoms is substantially affected by the initial ratio of the reactants. In the experiments, where all of the NO was introduced through the 2nd injector, the overall yield of atomic iodine was nearly 100 % (related to HI) at NO:ClO_2 ≅ 1 or 1.5 (see **Fig. 16**. A substantially lower yield (70 and 45 %, respectively) was obtained with NO:ClO_2 ratios equal to 2 and 2.5. This effect can be explained by a different mechanism of Cl atom formation for the different experimental conditions. At NO:ClO_2 ≥ 2, chlorine atoms are formed very rapidly by the chain branching mechanism and their fast recombination occurs before HI admixing. This takes place in the regions with an excess of ClO_2 and NO, and insufficient HI concentration.

In the case of the smaller ratio NO:ClO_2 ≅ 1, more stable ClO radicals are formed being in equilibrium with Cl atoms and formed ClOO radicals. Our previous modeling results have

shown[2] that the formation of atomic chlorine by the chain mechanism prevails at $NO/ClO_2 \cong 2$ and proceeds much faster than the non-chain process, which occurs predominantly at $NO/ClO_2 \cong 1$. In a real system with a limited rate of Cl and HI mixing, the first case is more effective because the loss processes of Cl atoms occur in the regions with insufficient HI concentration.

In some experiments, the order of NO and HI injection into the primary ClO_2 flow was reversed. A more uniform HI concentration in the region of NO admixing was expected and consequently, regions with fast generation of Cl atoms and insufficient HI concentration might be minimized. This could reduce the recombination loss of Cl atoms. On the other hand, some ClO_2 and HI might be consumed by the direct formation of molecular iodine. When HI (10-220 μmol s^{-1}) was injected into the primary flow with ClO_2 (240 μmol s^{-1}), and NO (280 μmol s^{-1}) was admixed 20 mm downstream, the rate of atomic iodine formation estimated by both detection techniques was about the same as in the case when NO was admixed 3.7 mm upstream the HI injector. Also in the configuration with two NO injectors, no significant difference in the iodine atom production between the "reverse order" (NO_I – HI – NO_{II}) and the "normal order" (NO_I – NO_{II} – HI) of injectors was found, if a short distance (3.7 mm) between the NO_{II} and HI injectors was maintained. Both arrangements are suitable for the effective generation of iodine atoms owing to a low loss of chlorine atoms.

In all experiments the gas temperature measured in the diagnostic cell was higher than the inlet temperature (20°C) due to exothermic reactions. A steep temperature rise was observed after ClO_2 was mixed with NO. The temperature rise was lower after HI admixing. The gas temperature in the diagnostic cell was between 80°C and 120°C.

3.1.1.2. Results of atomic iodine generation in flow of singlet oxygen

Further experiments were performed with chemically generated atomic iodine in the presence of a singlet oxygen flow. Gas exiting the singlet oxygen generator (not diluted with any buffer gas) was introduced into the iodine reactor as a primary flow. In first experiments, ClO_2 diluted with nitrogen was introduced through the first injector, NO through the second injector, and HI through the third injector. Nitrogen was introduced into the reactor only in mixtures with ClO_2, NO, and HI, respectively. In the experiment with a short distance (10 mm) between the HI injector and the ISD cell, the formation rate of atomic iodine

detected by both experimental methods was nearly the same regardless of the $O_2(^1\Delta)$ presence (see **Table 3**).

Tab. 3

Generation of atomic iodine either in nitrogen or a mixture with singlet oxygen. Primary flow: no or $O_2(^1\Delta_g)$ +$O_2(^3\Sigma_g)$, 1st injector: 130 μmol ClO_2 s^{-1}+1.25 mmol N_2 s^{-1}, 2nd injector: NO+N_2 , 3rd injector: HI+N_2, $d_{2\text{-}3}$ = 3.7 mm

$d_{3\text{-ISD}}$, mm	n_{N2}^{tot}, mmol/s	$n_{O2(\Delta)}$, mmol/s	$n_{O2(\Sigma)}$, mmol/s	n_{NO}, μmol/s	N_{HI}, μmol/s	n_I^{ISD}, μmol/s	n_I^{VIS}, μmol/s
10	4.2	-	-	166	145	22	70
10	4.1	0.39	1.9	166	135	20	70
33	4.6	-	-	159	155	5	70
33	4.5	0.39	1.9	159	145	24	70

It appears that the $O_2(^1\Delta_g)$ did not change the rate of atomic iodine generation. At a longer distance (33 mm) between the HI injector and the ISD cell, a substantial fraction of the iodine atoms in the nitrogen flow recombined upstream the ISD cell. This was gleaned from the fact that the ISD signal was 4.4 times lower than in the previous case. In the presence of singlet oxygen, this signal increased 4.8 times due to I_2 dissociation by $O_2(^1\Delta_g)$. The overall flow rate of atomic iodine (**n_I^{VIS}**) was the same in all cases. The observed production of atomic iodine in the ground state even in the presence of $O_2(^1\Delta)$ was explained by a low $[O_2(^1\Delta)]/[\text{total } O_2]$ ratio in the reactor (about 15 – 20 %) which was near the threshold value necessary for population inversion in atomic iodine. This low ratio was caused by a high $O_2(^1\Delta)$ quenching loss upstream the iodine reactor due to a high pressure loss in the reactor (and consequently a high pressure between the jet SOG and the reactor), and the absence of diluting gas. The reason for this high pressure was the small cross-section of the reactor (0.59 cm^2), and the high flow rates of secondary gases.

A substantial reduction in $O_2(^1\Delta)$ loss was achieved by introducing the ClO_2 and N_2 mixture into the $O_2(^1\Delta)$ flow close to the generator exit, instead of into the reactor through the 1st injector. The volume between the $O_2(^1\Delta)$ generator and the iodine reactor was also reduced, and the flow rates of the other reactants were reduced to minimize the pressure loss inside the iodine reactor. These modifications helped to increase the $O_2(^1\Delta_g)$ yield to 40 - 45 % at the iodine reactor entrance. Under these conditions, gain on the 3 - 4 hyperfine transition in the iodine atom was observed (see curve 1 in **Fig. 17**). The curve 2 in **Fig. 17** represents the

absorption curve recorded with similar flow rates of reactants but with no $O_2(^1\Delta_g)$ in the primary flow.

In the experiments with atomic iodine in the nitrogen flow, the evaluated gas temperature in the ISD cell was 81±13°C. The temperature was calculated from the Gaussian width after the deconvolution of the Voigt profile of the absorption-frequency curves. The temperature of 58°C in the diagnostic cell located downstream was measured by a thermocouple. In a flow of $O_2(^1\Delta)$, the temperature in the ISD cell was 117 ± 22°C, and the temperature measured by the thermocouple in the diagnostic cell was 180°C. The temperature increase in the flow direction observed in this case may be ascribed primarily to the exothermic quenching of I^* atoms by water molecules. Further processes that can lead to higher temperatures in the $O_2(^1\Delta)$ experiments are the $O_2(^1\Delta)$ self-quenching and pooling reactions.

3.1.2. Investigation in the small-scale reactor with probe beam perpendicular to gas flow

A reactor was designed in order to have possibility to measure a concentration gradient of generated atomic iodine downstream of the reactor. Owing to some necessary optical path of the diagnostic beam, and for the sake of saving the reactants (mainly HI), the gas velocity through the detection cell was low (40 m/s). The inner width at the cell was 25 mm and height 8 mm. Technical drawing of the reactor and the detection cell with two side wedge-shaped windows is in **Fig. 18**. The primary gas from the jet SOG after mixing with ClO_2 and passing the $O_2(^1\Delta_g)$ detection cell was introduced through the tube with a quick coupler 1 into the reactor. The NO + nitrogen mixture was introduced by the injector 2 with two rows of holes, and HI by two injectors 3. The parameters of injectors were calculated so to assure a full penetration of secondary gases into the primary gas: the NO injector with two rows of holes of 0.4 mm i.d., 23 holes in each row, and the distance between nearby holes 1 mm. In one type of the NO injector, both rows of holes were oriented in vertical direction (up and down), in the second type of this injector, the NO streamed from the first row of holes under 45^o and from the second row of holes under -45^o to the horizontal direction. Each of both HI injectors had 9 holes of 0.4 mm i.d. in one row. A time delay within 0–177 microseconds between NO admixing into ClO_2 flow, and following HI admixing could be changed by exchanging the NO injectors and orientation of HI injectors, corresponding to a change of the distance between holes of NO and HI injectors within 0–7 mm (in the gas flow direction).

The diode probe beam passed through the reaction mixture and two side wedge-shaped windows 4 perpendicularly to the gas flow. The probe beam emitter/detector unit, and mirror system for beam alignment of the ISD were mounted on assembly of motorized linear positioning equipment (see **Photo 1 a, b**). The probe beam could be moved along the path distant minimally 12 mm and maximally 55 mm from the axis of HI injectors. A jacketed thermocouple Ni-CrNi of 1 mm i.d was inserted into the tube 5 for measuring the gas temperature. A flange connects the reactor body with the diagnostic cell containing the optical cell for I_2 detection by means of absorption photometry at 488 nm.

3.1.2.1. Results and their discussions

Atomic iodine generation in excess of nitrogen

The atomic iodine concentration (molar flow rate, respectively) in dependence on a distance from HI injection was measured in this reactor. An example of this course, obtained at a distance between NO and HI injectors of 7 mm is shown in **Fig. 19** (I atoms detected by the diode probe diagnostics). It can be seen that the flow rate of atomic iodine decreased from its maximum value at a distance of 15 - 20 mm from the HI injector. This is caused by recombination of I atoms, which is accelerated mainly by the presence of NO_2 in this reaction system. It can be supposed that decrease in atomic iodine could be substantially slower in the COIL conditions owing to a lower pressure and higher gas velocity (by about one order) in comparison with the velocity of 40 m/s in the small-scale reactor. Measured values of I concentration in this experiment ($6 \div 12 \times 10^{14}$ cm^{-3}) are comparable with concentrations typical for the cavity in the supersonic COIL. The gas temperature in this experiment was ~350 K, which is about 100 K higher then in the COIL cavity due to the absence of the supersonic cooling in this device.

The production of atomic iodine was higher when the distance between NO and HI injectors was shorter (3.5 mm ~ 90 μs) even at lower flow rates of reactants (see **Fig. 20**). In this experiment and all others as well, the measured values of I concentration were the same during the probe beam moving in forward and backward directions. This proved a time stability of atomic iodine production. The gas temperature evaluated by the know procedure from the Gaussian width of the recorded curves (see **Fig. 21**), slightly declined with a distance along the flow.

The highest production rate of atomic iodine was attained at the smallest distance between NO and HI injection, i.e, when both reactants were injected simultaneously against

each other (see **Fig. 22**). It was further found that the production rate of atomic iodine did not increased proportionately with increasing flow rate of reactants. This is documented in **Fig. 23** when ClO_2 flows rates were twice higher, and HI flow rate three times higher then in **Fig. 22**. This result is in agreement with the results in **Fig. 12** obtained in the former reactor, where the overall rate of production of atomic iodine, estimated indirectly from I_2 concentration, increased proportionally with the HI flow rate, while the I production was much lower when I was detected by ISD. The maximum production region was probably shifted upstream the ISD cell. This assumption was confirmed by a faster decline of I flow rate along the flow axis in **Fig. 23**. The atomic iodine yield up to 88 % was obtained at lower flow rates of reactants (see **Fig. 24**).

Atomic iodine generation and excitation in $O_2(^1D_g)$ flow

Atomic iodine was generated at the same flow rates of reactants as in nitrogen (see **Fig. 24**), only singlet oxygen (560 μmol/s) from the jet SOG was introduced as a primary flow. The $O_2(^1\Delta_g)$ yield determined in the $O_2(^1\Delta_g)$ optical cell was 48 %, and the ratio of atomic iodine flow rate (in nitrogen) to singlet oxygen was ~4 % corresponding with the COIL conditions. The measured dependence of $n_{I^*\text{-}I/2}$ on a distance of the HI injector in flow direction (see **Fig. 25**) showed that the concentration of excited I^* decreased rather fast. Evaluated concentrations of I^* are also several times lower then follows from the equilibrium equation of the pumping reaction: $[I^*]/[I] = 0.75 \exp[(401.4/T)\ [O_2(^1\Delta_g)]/[O_2(^3\Sigma)]$. In order to reveal the reason for this, the 1-D modeling of this reaction system was performed for conditions of the above experiment. This model involved, except the rate constants of atomic iodine production reactions and pumping reaction (given in the Report 0002 of this contract), the known rate constants for I^* quenching by the following reaction components: I_2 ($1.6\text{x}10^{-11}$ $\exp(272/T)$ cm^{-3}), $O_2(^3\Sigma)$ ($3.1\text{x}10^{-8}/T$ $\exp(-403/T)$ cm^{-3}), H_2O ($2\text{x}10^{-12}$ cm^{-3}), $O_2(^1\Delta_g)$ ($4\text{x}10^{-24}$ $T^{3.8}$ $\exp(700/T$ cm^{-3}), N_2 ($2\text{x}10^{-16}$ cm^{-3}), Cl ($2\text{x}10^{-10}$ cm^{-3}), and Cl_2($8\text{x}10^{-15}$ cm^{-3}). The quenching constants for HI ($5\text{x}10^{-14}$ cm^{-3}), and HCl ($6.5\text{x}10^{-15}$ cm^{-3}) were omitted for their small values. It followed from this modeling that the measured decrease in I^* concentration with the flow coordinate was higher then the calculated one. A relatively good agreement between measured and calculated values was achieved under the assumption that atomic iodine is quenched also by some species with the quenching constant of about $1\text{x}10^{-11}$ cm^{-3} assuming that its concentration is the same as HCl. The species responsible for the fast I^*

quenching may be, e.g., NOCl or NO_2Cl, either in the ground or the excited state. In these considerations, one should take into account that the gas temperature was much higher in these experiments (up to 450 K) then the room temperature for which the most of the used quenching constants was published. The high temperature under these experimental conditions is caused by exothermic reactions, mainly the self-quenching and pooling reactions of $O_2(^1\Delta_g)$, and I^* quenching by H_2O at considerable concentrations of these component, and the absence of isentropic cooling of the gas like in the supersonic COIL. Measured dependence of the gain on the distance from HI injector is given in **Fig. 26**.

These results obtained on the modified small-scale device showed that the production of atomic iodine in non-reactive nitrogen was very effective and can be realized also in environment of reactive singlet oxygen where I^* quenching rate is however substantially increased by some unknown processes. It might be anticipated that this atomic iodine generation would be constant along the flow in the COIL conditions where the gas velocity is much higher and temperature lower that in the pilot device. This was the reason for the next experiments with atomic iodine generation directly in the COIL device.

3.1.3. Investigation of atomic iodine generation in the COIL device

The results and experience obtained during systematic investigation of atomic iodine generation on both types of pilot small-scale devices described above were utilized for a design of experimental investigation of this process directly on the supersonic COIL device. Some constructional modifications of the conventional COIL, from which I_2 system was removed, were needed, particularly a new gas management and injection of reactants. The primary flow from the jet SOG flew through the ClO_2 injector and then the optical diagnostic cell for $O_2(^1\Delta_g)$ detection. Mixture of ClO_2 + N_2 was introduced into the subsonic channel through the injector in the form of a tube (6 mm o.d.) located horizontally in the centre of the channel. The 25 holes of 0.7 mm in two rows in the injector were oriented $\pm 45^o$ to the main flow. Then the gas entered the channel in the NO+HI injector body (see **Fig. 27**). It contains two rectangular tubes 1 for NO+N_2 injection, and two tubes 2 for HI+N_2 injection. Each tube of NO injector had 33 holes of 0.7 mm in the first row and 32 holes of 0.5 mm in the second row. Each tube of HI injector had 25 holes of 0.7 mm in one row and 24 holes of 0.5 mm in the second row. A distance between the first and second rows of NO and HI injectors was 2.5 mm, and between the second row of NO injector and the first row of HI injector was 3 mm.

The number and diameter of holes were calculated to assure an optimal penetration of secondary gases into the primary gas for the following flow conditions:

Primary gas: 36 mmol O_2/s + 80 mmol He/s + 4 mmol Cl_2/s + 2.5 mmol ClO_2/s + 25 mmol N_2/s

The 1st injector: 5 mmol NO/s + 45 mmol/s, the 2nd injector 2.5 mmol HI/s + 25 mmol N_2/s

These experimental conditions were counted for He as a buffer gas in the primary gas because the jet SOG was also designed for this gas. Reagents for atomic iodine production are, however, diluted by nitrogen because these mixtures were available.

3.1.3.1.Results and their discussion

A few preliminary experiments were performed so far, during which the vacuum system with low suction rate (1000 m^3 s^{-1}) was used because the main vacuum complex (Ruta 3000 m^3h^{-1}) was out of order. The gas velocity in subsonic channel was estimated ~230 m/s, and 564 m/s in the cavity. In the experiments described below, the distance of the second row of holes of HI injector from the nozzle throat was 3.5 mm An example of time dependence of atomic iodine production at a distance of 39 mm, and during the following probe beam shift along the cavity is shown in **Fig. 28**. The dependence of I flow rate on the distance from nozzle throat is shown in **Fig. 29**. It is obvious from **Fig. 28** that the rate of atomic iodine production decreased with decreasing HI flow rate, and therefore one could supposed that the rate of I production should be constant at a constant HI flow. In the next experiments, the HI flow rate was varied up to 1.76 mmol s^{-1}, and the rate of atomic iodine production did not exceed 1 mmol s^{-1} (measured by ISD). The yield of atomic iodine related to HI or ClO_2 was 40–60 %. The concentration of produced atomic iodine in the optical resonator was within (3÷12) x 10^{14} cm^{-3}. This is comparable with I concentrations in the conventional COIL.

Conclusions from this investigation

Three types of reactors and equipment were designed and tested.

a) Experiments on the pilot reactor with probe beam coaxial with gas flow

- Appropriate experimental arrangement and suitable conditions for effective production of atomic iodine like the distances between injectors of reactants and reactants flow rates were found.

- High yield of atomic iodine (50-95%) in non-reactive environment (nitrogen) was obtained.
- Generation of atomic iodine was achieved also in reactive environment with singlet oxygen.
- Gain on $I(^2P_{1/2}) - I(^2P_{3/2})$ transition in this system was proved.

b) Experiments on the pilot reactor with probe beam perpendicular to gas flow

- In excess of non-reactive nitrogen and at low gas velocity (40 m/s), a concentration course of atomic iodine along the flow was measured at different experimental conditions.
- Measurements performed in $O_2(^1\Delta_g)$ stream showed a remarkable gain decrease along the flow. This was explained by presence of some species responsible for rather fast quenching of I^*. This quenching effect might be intensified by the high gas temperature (450 K) caused by exothermic processes in these experimental conditions due to absence of isentropic gas cooling.

c) Experiments on I generation in COIL

- Preliminary experiments on I generation in the COIL device in nitrogen flow proved the effective production of atomic iodine in the supersonic flow conditions.
- Concentrations of produced atomic iodine attained values that are typical for a conventional COIL operation.
- No significant decrease in I concentrations along the flow in the cavity was observed.
- It can be supposed from these results that the generation of atomic iodine in flow conditions typical for supersonic COIL would be possible with relatively high yield and after further optimization of experimental conditions (flow rates of reactants and distances of injectors from the nozzle throat).

3.1.4. 2-D modeling of some problems during atomic iodine generation

Two partial problems connected with the experimental investigation of atomic iodine production were modeled:

1) The reacting flow inside the previous version of the optical cell for Iodine Scan Diagnostics (ISD)

2) The mixing and reaction between parallel flows of chlorine dioxide (ClO_2) and nitrogen monoxide (NO) in nitrogen buffer gas.

3.1.4.1. Modeling of flow inside ISD cell

Several preliminary simulations were performed to get experience with the 2-D modeling computer code. In these simulations, the influence of the geometry, number of species, choosing different physical models, etc. on the behavior of the flow, and a convergence of the solution was particularly studied. After that, the real geometry and the appropriate chemical composition were considered for next simulations.

Description of the problem

In this chapter, the optical cell with the ISD beam parallel with the gas flow downstream of the reactor for atomic iodine generation is modeled. This arrangement was first used where the ISD cell was connected with the reactor through a tube of 20 mm long.

The physical domain consists of three 10 mm i.d. stainless tubes that were rectangular connected, the middle of which serving as the ISD optical cell. A longitudinal cross-section of this domain is considered as a computational domain for the simulation. The premixed flow of atomic chlorine and hydrogen iodide diluted with nitrogen flows through the inlet tube from the left; atomic iodine is formed and subsequently recombined to iodine molecules. The resulting mixture is pumped out through the right tube. The computational domain is divided into 5984 small cells (see **Fig. 30**)

Based on the preliminary simulations, the flow is assumed to be laminar and steady. The mixture is treated as a viscous, compressible, ideal gas. The chemical reactions are modeled by the finite rate chemistry (see **Table 4**), and a molecular diffusion is simplified by using the Fick's law.

Input parameters, boundary conditions

The values are summarized in **Table 5**. The solution is marched so that the total mass flux and outlet pressure (taken from the measurement) are constant. The composition of the inflow mixture is based on the previous 1-D calculation of the reaction between ClO_2 and NO (see the reaction scheme in Rep. 001 of this contract). This calculation was made for the flow rates: 220 μmol ClO_2 s^{-1}, 375 μmol NO s^{-1}, 27.5 μmol Cl_2 s^{-1}, and 5750 μmol N_2 s^{-1} using the volume flowrate 8 l s^{-1}. The mixture composition was considered for the reaction time when

all ClO_2 was consumed. The input to the domain formed the mixture of 220 μmol HI s^{-1} with 2530 μmol N_2 s^{-1} added to above mixture.

Tab. 4

Reactions for modeling of flow inside ISD cell

Cl + HI ? HCl + I	$2.31x10^{-8}(T/298)^{-4.45}exp(-12472/8.314/T)$
Cl + NO_2 + N_2 ? NO_2Cl + N_2	$1.3x10^{-30}(T/298)^{-2}$
NO_2Cl + Cl ? Cl_2 + NO_2	$5.5x10^{-12}$
I + NO_2 + N_2 ? INO_2 + N_2	$3.01x10^{-31}(T/298)^{-1}$
INO_2 + I ? I_2 + NO_2	$8.3x10^{-11}$
I + I + I_2 ? I_2 + I_2	$2.68x10^{-31}(T/298)^{-3.06}exp(6568/8.314/298)$
Cl + Cl + N_2 ? 2Cl + N_2	$1.6x10^{-33}$ exp(6693/8.314/T)
I + I + N_2 ? I_2 + N_2	$6.15x10^{-34}(T/298)^{0.07}exp(7433/8.314/298)$

Tab. 5

Input and boundary conditions for modeling of flow inside ISD cell

Input	Total flux	3.909 kg/m^2/s
	Composition (w/w)	Cl 0.128
		ClO 0.124
		Cl2 0.078
		HI 0.0917
		NO 0.0013
		NO_2 0.0533
		N_2 0.821
	Temperature	400 K
Output	Pressure	3251 Pa (24 torr)
Wall		No slip, 400 K

The values of thermodynamic and transport data for the relevant species were taken from the NIST Chemistry Webbook[3] and NASA Technical Report.[4] Heat capacity and viscosity data were temperature-dependent, based on the polynomial fit of the published data.

Results and discussion

The solution was terminated by 2000 iterations when the residuals fell down under 10^{-4}, except of the continuity equation (10^{-3}) and energy equation (10^{-5}). The average concentration of atomic iodine was fluctuating in the range of 10 % during last 300 iterations.

The velocity vectors are illustrated in **Fig. 31**. A presence of two large vortexes at both ends of the optical cell is apparent, as well as two small vortexes downstream of the sharp edges. The flow is narrowing down and accelerating from the initial velocity 85 m s^{-1} to 243 m s^{-1}. These facts are important for the interpretation of the measurement of atomic iodine concentration in a real ISD cell. The probe laser beam passed the optical cell parallel to the flow, and reflected by the Au mirror it returned back. The diameter of the beam was 2.5 mm, while the diameter of windows of the optical cell was 10 mm, so the position of the beam with respect to the tube wall could be varied. It can be seen in **Fig. 32**, showing the contours of atomic iodine mass fraction, that the detected concentration is very sensitive to the probe beam alignment. A maximum concentration is attained already before the entrance into the optical cell and then only a recombination of I atoms to I_2 molecules proceeds. The decrease in atomic iodine concentration and high inhomogeneity along the optical path affected the measured concentration values. It follows from the calculations, that these values could reach from 30 to 65 % of the maximum local I atom concentration. These fractions are substantially higher than the fraction obtained by 1-D modeling (premixed model) (see **Fig. 13**), and corresponding better to experimental data.

Among other simulation results, the temperature field is interesting (see **Fig. 33**). The maximum temperature of 430 K is located in the region of the second large vortex, which is a result of an exothermic recombination of atomic iodine.

The pressure drop between the inlet and outlet resulting from the simulation is 1.8 kPa. This value is highly over-estimated (the calculation using the friction loss coefficients gives the value of 0.5 kPa) and is probably caused by a relatively strong reduction of the circular-like shape to the two-dimensional shape.

3.1.4.2. Modeling of mixing and reaction between ClO_2 and NO in nitrogen flow

An analysis of characteristic times for diffusion (80 μs) and reaction (10 μs) in the process of atomic chlorine production shows the important effect of the diffusive mixing. In order to evaluate this effect on the overall process, the mixing and reaction of a thin jet of NO with parallel stream of ClO_2 was simulated by means of 2-D model.

Description of the problem

Dimensions of the physical domain are derived from those of the ISD diagnostic cell in another experimental arrangement (see **Fig. 18**). For simplicity, two jets of NO propagate

from the top and bottom wall and bend to the parallel streams. The bent regions are not modeled; it is assumed, that the flow enters parallel to the main stream. The computational domain is shown in **Fig. 34**, and only one half of each jet is modeled. The computational mesh consists of 15080 cells. The flow is assumed to be laminar and steady. The mixture is treated as a viscous, compressible, ideal gas. The chemical reactions are modeled by the finite rate chemistry (see **Table 6** for rate constants), molecular diffusion is modeled by means of exact Stefan-Maxwell multicomponent diffusion equations.

Tab. 6

Reactions for modeling of mixing NO and ClO_2

$ClO_2 + NO$? $ClO + NO_2$	$2.51x10^{-12}$ exp(-4989/8.314/T)
$ClO + NO$? $Cl + NO_2$	$6.39x10^{-12}$ exp(2411/8.314/T)
$Cl + ClO_2$? 2 ClO	$3.40x10^{-11}$ exp(1330/8.314/T)
$Cl + NO_2 + M$? $NO_2Cl + M$	$1.3x10^{-30}$ (T/298)^(-2)
$ClO + NO_2 + M$? $NO_3Cl + M$	$3.69x10^{-33}$ exp(9562/8.314/T)
$Cl + NO_2Cl$? $Cl_2 + NO_2$	$5.5x10^{-12}$
$Cl + NO + M$? $NOCl + M$	$1.8x10^{-32}$ exp(4423/8.314/T)
$Cl + NOCl$? $Cl_2 + NO$	$6.59x10^{-11}$ exp(-1054/8.314/T)
$ClO + ClO$? $Cl + ClOO$	$3.01x10^{-11}$ exp(-20370/8.314/T)
$ClOO + M$? $Cl + O_2 + M$	$2.81x10^{-10}$ exp(-15132/8.314/T)
$Cl + ClOO$? 2 ClO	$1.2x10^{-11}$
$ClO + ClO + M$? $Cl_2 + O_2 + M$	$1.0x10^{-12}$ exp(-13220/8.314/T)
$Cl + Cl + M$? $Cl_2 + M$	$1.0x10^{-33}$ exp(6693/8.314/T)

Input parameters, boundary conditions

The values are summarized in **Table 7**. Two different simulations were performed for the flowrate ratio $NO:ClO_2$ = 1:1 and 2:1, respectively. The values of thermodynamic and transport data were taken from the NIST Chemistry Webbook[3] and NASA Technical Report[4]. For simplicity, heat capacity and viscosity data were kept constant at 300 K, except for nitrogen buffer gas, where the temperature dependence was based on the polynomial fit of the published data.

Tab. 7

Input and boundary conditions for modeling of mixing NO and ClO_2

Input	ClO_2 flux	0.1831 kg/m^2/s 25 μmol ClO_2/s + 1250 μmol N_2/s
	NO flux	2.609 kg/m^2/s 25 or 50 μmol NO/s + 225 or 450 μmol N_2/s
	Temperature	300 K
Output	Pressure	1000 Pa
Wall		No slip, 300 K
Jet centerline		Symmetry conditions

Results and discussion

Contours of mass fraction of atomic chlorine (Cl) and ClO radical for the ratio NO:ClO_2 = 1:1 are shown in **Figs. 35 a, b** A diffusive character of mixing can be seen, which is completed on the path of 25 mm (not shown). Atomic chlorine is located mostly in the bottom half of the channel, 4.5 mm downstream from the inlet, while ClO is located near the upper wall, 5 cm downstream from the inlet. Using the calculated average velocity of 40 m/s, the maximum production rate of Cl atoms is 17 μmol s^{-1}, and 26 μmol s^{-1} of ClO radical. In comparison with 1-D calculation that is shown in **Fig 37,** a very good agreement was in the case of ClO (25 μmol s^{-1} in 1-D model), but the "2-D production rate" of Cl is 7 times higher then 1-D production rate (2.5 μmol s^{-1}).

The mass fraction contours for the ratio NO:ClO_2 = 2:1 are shown in **Figs. 36 a, b** In contrary to the previous case, Cl is located mostly in the upper part of the channel, but at the same flow distance like in the "1:1" case. The maximum concentration of ClO is attained at shorter reaction path (3 mm) then in the "1:1" case. The maximum production rates are 25 μmol Cl s^{-1} and 28 μmol ClO s^{-1}. As can be seen in Figure I, the 1-D maximum production rates are significantly lower.

A different results between two ratios of NO:ClO_2 in 1-D modeling was explained previously by the different reaction mechanism.[5] At the ratio NO:ClO_2 = 1:1, the process goes predominantly via non-chain mechanism where ClO is mostly produced by reaction 1 (**Tab. 6**). At the ratio 2:1, there is a sufficient amount of NO to produce Cl, although, thanks to the chain mechanism, ClO is formed as well. The deviation from this behavior, observed in 2-D simulation, can be ascribed to a local excess of NO caused by its relatively high concentration in the narrow jet. It is apparent from the **Figs. 37** and **38** that the places of maximum

concentration of Cl and ClO are located at approximately twice longer path in 1-D result then in 2-D simulation. This substantial difference can be also a reason of the high concentration gradient at the jet boundary connected with the fast chemical reactions.

Conclusion from this modeling

These results are a good base for both the modeling and design of experiments concerning the subsequent injection of HI. The 2-D model predicts relatively small localization of Cl in longitudinal and vertical direction. A correct description of the penetration of transverse jet into the main flow is, however, impossible by 2-D model. In order to predict the reaction of HI with Cl, the 3-D model would be necessary.

3.2. Investigation of atomic iodine generation via F atoms

3.2.1. 1-D modeling of atomic iodine generation by chemical reaction of F_2 + NO + HI

Detail description of the reaction system and results of 1-D modeling was presented in the interim Reports 0001 and 0002 of this contract. Main results and conclusions following from this modeling for the experimental investigation are given below.

The kinetics of the overall system can be then described by the following set of reactions.

F atoms generation:	$F_2 + NO \rightarrow F + NOF$	$k_1 = 7 \times 10^{-13} e^{(-1150/T)}$	(1)
F atoms consumption:	$F + NO + He \rightarrow NOF + He$	$k_2 = 1.1 \times 10^{-31}$	(2)
	$F + F + He \rightarrow F_2 + He$	$k_3 = 5.3 \times 10^{-34}$	(3)
	$F + NO + NO \rightarrow NOF + NO$	$k_4 = 1.7 \times 10^{-31}$	(4)
	$F + I_2 \rightarrow IF + I$	$k_5 = 4.3 \times 10^{-10}$	(5)
I atoms generation:	$F + HI \rightarrow I + HF$	$k_6 = 1.512 \times 10^{-10} e^{(-5057.8/RT)}$	(6)
I atoms consumption:	$I + I + He \rightarrow I_2 + He$	$k_7 = 3.8 \times 10^{-33}$	(7)
	$I + I + I_2 \rightarrow I_2 + I_2$	$k_8 = 3.7 \times 10^{-30}$	(8)
	$I + NO + He \rightarrow INO + He$	$k_9 = 5.5 \times 10^{-33}$	(9)
	$I + INO \rightarrow I_2 + NO$	$k_{10} = 2.6 \times 10^{-10}$	(10)
	$I + F_2 \rightarrow IF + F$	$k_{11} = 1.9 \times 10^{-14}$	(11)

The processes (2) to (5) describing loss-processes of F atoms are suppressed substantially by a fast competitive reaction (6) of fluorine atoms with hydrogen iodide. This effect is most important in the case of simultaneous mixing of all three gases, F_2, NO and HI in one place of

the reactor. The flow rates of reactants were chosen so that the flow rate of produced atomic iodine is sufficient for operation of 1 kW-class supersonic COIL, i.e. 2 to 3 mmol I s^{-1}.

The 1-D modeling was performed for adiabatic conditions, with neglecting the heat transfer to the walls and assuming instantaneous mixing. Dilution of F_2 and NO with helium was considered in calculations the same as it is available in commercial gas bottles, i.e., 5% F_2 in He, 20% NO in He, and pure HI. The flow rates of reactants, pressure and initial temperature of reaction mixture considered in calculations are listed in the **Table 8.** The calculations were performed for different helium dilution and total pressure including conditions that characterize the subsonic region (i.e., the gas flow upstream of the nozzle throat) of our 1kW-class supersonic COIL.

Tab. 8

F_2	5 mmol/s
NO	5-10 mmol/s
HI	5 mmol/s
He	45-205 mmol/s
Pressure	5-20 kPa
Initial temperature	300 K

Generation of F atoms

The production of F atoms was modeled including the reactions (1) - (4) for several values of initial pressure, helium dilution and initial concentration ratio [NO]:[F_2]. The results are summarized in **Table 9**.

Tab. 9
Production of F atoms.
$h_F = n(F)_{max}/n(F_2)_0$ - maximum conversion of F_2 to F; *T, p, t* - resultant values of temperature, pressure, and reaction time at the place of maximum conversion

[NO]:[F_2]	p_0(kPa)	[He]:[F_2]	h_F	T (K)	p (kPa)	τ (ms)
2	1	23	0.70	490.6	1.44	4.0
2	2	23	0.50	514.3	2.55	1.7
2	4	18	0.41	586.7	4.64	0.6
1	4	23	0.34	517.8	4.43	3.2
2	4	23	0.35	536.6	4.48	0.7
2	4	41	0.24	442.4	4.23	1.3
2	10	23	0.20	564.9	10.27	0.2

It is obvious that the conversion of F_2 molecules to F atoms rapidly decreases and the reaction path becomes shorter with increasing in the initial pressure of reaction mixture. The conversion substantially declines with increasing helium dilution ratio because the rates of the reactions (2), (3) and (1) increase. The conversion is not influenced by the initial ratio [NO]:[F_2] but a significant amount of NO remains non-reacted at [NO]:[F_2] > 1.

The concentration profiles of reactants and reaction products calculated for conditions typical in the subsonic part of the COIL (4 kPa) are shown in **Fig. 39.** The yield of F atoms did not exceed 17 % (conversion of F_2 to F was 0.35) under these conditions. In accordance with the previous modeling[2], the production of F atoms is very slow. Assuming the gas velocity of 200 m s^{-1}, HI should be introduced into the flow channel at the place of maximum [F], which is at a distance of 20 cm downstream from the F_2/NO injection. A generation of F atoms in a separate reactor and its injection together with HI into the $O_2(^1\Delta_g)$ flow could be another possibility.

Generation of I atoms

The recent modeling showed that simultaneous mixing of F_2, NO, and HI provides promising results on the efficient production of atomic iodine. In this case, hydrogen iodide reacts instantly with formed F atoms, and reduces the rate of loss reactions (2) and (3). The modeling included the set of reactions (1) - (11). The results are summarized in **Table 10.** The effect of helium dilution on the conversion of F_2 to I atoms is very small on the contrary to the F atoms generation. The conversion is higher by 20 % at the initial concentration ratio [NO]:[F_2] = 2:1 against 1:1. The time course of concentrations for the initial pressure of 4 kPa is shown in **Fig 40**. A pressure dependence of the F_2 to F conversion (in the system F_2+NO) and F_2 to I conversion (in the system F_2+NO+HI) is shown in **Fig. 41**, from which can be seen that F atoms conversion rapidly decreases with increasing pressure, while the conversion to I atoms is less pressure dependent.

The gas temperature did not exceed 550 K in the case of F atoms production, and 700 K in the case of I atoms production at the dilution ratio He/F_2 up to 36. The ratio [F_2]:[He] = 1:30 corresponds to the He that is contained in the COIL primary gas.

Tab. 10
Production of I atoms.
$h_I = n(I)_{max}/n(F_2)_0$ - maximum conversion of F_2 to I*; T, p, t* - resultant values of temperature, pressure and reaction time at the place of maximum conversion.

[NO]:[F_2]	p_0(kPa)	[He]:[F_2]	h_I	T (K)	p (kPa)	τ (ms)
2	1	9	0,86	1373	1.00	5.5
2	1	18	0.88	976	1.00	5.8
2	1	36	0.89	692	1.00	9.9
1	1	37	0.68	611	1.00	10
2	4	36	0.84	652	4.57	1.5
2	10	36	0.64	642	10.0	0.5

Generation of I^* state in this system

The above results on the F and I atoms generation were included into calculations of I^* population in the stream of singlet oxygen. The 1-D modeling of reactions between primary and secondary gases in COIL can describe the real processes only approximately because it cannot meet all mixing phenomena, nevertheless, these results presented below can provide first estimation of this process from the kinetic point of view with an emphasis on I^* atoms lifetime in the reaction system. The reactions between F, HI and $O_2(^1\Delta_g)$ were modeled in the first series of solution, and the reaction between I and $O_2(^1\Delta_g)$ in the second series of solution. The mixture resulting from the F and I atoms generation was assumed as the secondary gas. The gas composition exiting the $O_2(^1\Delta_g)$ generator in our COIL ([O_2]:[He] = 1:2, [$O_2(^1\Delta_g)$] : [$O_2(^3\Sigma_g)$] = 3:2, and 3% of H_2O) was considered as a primary gas. The reactions relevant to the system of $O_2(^1\Delta_g)$, I, and I_2 were taken from the reference of Paschkewitz *et al*.[6]

The subsonic mixing of F + HI + $O_2(^1\Delta_g)$ or I + $O_2(^1\Delta_g)$ (see **Figs. 42 a, c**) was considered at the initial pressure of 4 kPa and temperature of 300 K. The initial pressure of 10 kPa was assumed in the separate reactor for F and I atoms generation, respectively. The supersonic mixing of the same species (see **Figs. 42 b, d**) was calculated at pressure of 0.5 kPa and temperature of 200 K in the cavity, and pressure of 1 kPa was assumed in the separate reactor for F and I atoms generation, respectively. A constant mixture temperature was presupposed, and the initial concentration ratio of F or I atoms and $O_2(^1\Delta_g)$ was taken from the typical ratio of [I_2]/[O_2] = 1:50 in the conventional COIL operation.

F + HI + $O_2(^1D_g)$ system

A time development of I^* atoms concentration in subsonic conditions is shown in **Fig. 43** (solid line). The concentration rises up to 0.13 ms and then slowly decreases. Assuming the average gas velocity of 200 m s^{-1}, the maximum concentration is attained at a distance of 2.6 cm from HI injection. The excitation rate of I atoms in supersonic conditions is very low (see **Fig. 44**, solid line), and assuming the gas velocity of 1000 m s^{-1}, the maximum I^* concentration is attained at a distance of 1 m from HI injection. According to these results, the subsonic injection of F atoms together with HI into the $O_2(^1\Delta_g)$ flow seems to be more advantageous.

$I + O_2(^1D_g)$ system

Time development of I^* concentration calculated for this reaction system in subsonic conditions is shown in **Fig. 43** (dashed line). The concentration rises up to 0.04 ms and then rapidly falls. Assuming the average gas velocity of 200 m s^{-1}, the maximum concentration is attained at a distance of 8 mm only from HI injection. In supersonic conditions, the concentration rapidly rises and attains its maximum value before 0.03 ms, which corresponds to a distance of 3 cm (see **Fig. 44**, dashed line). Then the concentration slowly decreases. For example, 80 % of the maximum value is attained at a distance of 38 cm from HI injection.

The suggested and described process for generation of atomic iodine in COIL introduces into the laser mixture many new species, that can quench I^* state and $O_2(^1\Delta_g)$, respectively. According to known values of the rate constants for $O_2(^1\Delta_g)$ quenching, the quenching effect of this species is rather weak. The known rate constants for I^* quenching by reaction components are given in **Table 11.**

A comparison of the quenching by different species calculated from the initial concentrations of reactants provides an interesting insight into I^* lifetime in this reaction system. The initial reaction rates divided by initial I^* concentration for $I + O_2(^1\Delta_g)$ system in subsonic and supersonic conditions are shown in **Fig. 45 a, b**. The most effective quenchers are IF and HF molecules. The above-mentioned values are valid only for ground electronic states of these molecules, the quenching of IF^* and HF^* are not available in the literature. The ground and excited NOF molecules could be also very effective quenchers of I^*, but the appropriate quenching constant is unknown as well.

The quenching effect of NO and F_2 is small, so the residual content of these species should not cause a serious problem. The above estimation of the quenching effect of different components of this reaction mixture is approximate, and final answer to this problem can provide only the experimental investigation of this reaction system.

Tab. 11
Quenching constants of I^* by components present in reaction system for I atoms generation [$cm^3\ s^{-1}$]

NO	5×10^{-17}
HI	5×10^{-14}
HF	3×10^{-12}
H_2O	2.3×10^{-12}
I_2	3.5×10^{-11}
F_2	5.0×10^{-14}
He	5.0×10^{-18}
IF	1.3×10^{-11}

3.2.2. Modeling of F_2/NO/HI mixture for conditions in a small-scale experimental device

The results of modelling of conditions that are considered for experimental verification of this reaction system on a small-scale pilot device are summarized bellow. Following from the above given conclusion of the modeling that the highest yield of I atoms can be achieved by the effective mixing of all three reactants in the same place of the device, a similar design of the reactor was proposed for the experimental investigation of atomic iodine generation via F atoms as we use for atomic iodine generation via Cl atoms. This reactor makes possible to mix the primary flow together with two secondary flows nearly in the same place. Further, the optimal penetration of the secondary flows may be attained together with the possibility of adjusting the order and time span between both secondary flows.

The modeling of the reaction system in the proposed reactor issued from the set of reactions (1) - (11), the pumping capacity of the used rotary pump (25 m^3/h), and the total pressure in the reactor of 3.5 and 8 kPa, respectively. The calculations considered the same dilution of F_2 by helium as in the commercially available mixture (only 5% F_2), a dilution of other reactants by helium was 50% NO, and 50 % HI. The results of modeling are given in **Table 12**.

These results showed that the yield of atomic iodine decreased with increasing total pressure in the reactor and with decreasing ratio NO/F_2. A time at which 50 % of generated atomic iodine is recombined to I_2, τ_{50}, 10 to 30 times longer than $\tau_{max,}$ i.e., a time for achieving the maximum concentration of atomic iodine.

Tab. 12

The yield of atomic iodine, initial and residual content of reactants and products, resultant temperature of reaction mixture at different pressure in reactor

P	n^o_{F2}	n^o_{NO}	n^o_{HI}	n^o_{He}	τ_{max}	η_I	n_I	n_{I2}	n_{F2}	n_{NO}	n_{NOF}	n_{IF}	T	τ_{50}
kPa	μmol/s				ms	%	μmol/s						K	ms
3	109	218	109	2725	3	42.6	93	1	2	117	101	9	801	70
3	121	121	1221	2783	6	37.2	90	1	6	22	99	20	814	170
5	182	364	182	4550	2	40.6	148	1	6	198	166	18	785	28
8	291	582	291	7275	1	38.1	222	3	12	317	265	30	773	12

P – total pressure in the reactor; n^o, the initial molar flow rate of reactants; n – molar flow rate of products at the time of maximum I atom yield; η_I – maximum yield of atomic iodine at τ_{max}; τ_{50} – the time when 50% of produced atomic iodine is recombined to I_2 molecules.

Conclusions from this investigation

- 1-D modeling provided data on F_2 conversion into F or I atoms as a function of initial pressure, dilution and concentration ratio of reactants.
- First results of modeling showed that this reaction system is able to provide F atoms on relatively long reaction path in subsonic mixing of all reactants in the supersonic COIL (about 50 cm at the gas velocity of 200 m s^{-1}).
- Simultaneous mixing of HI and F_2/NO suppressed the loss processes of F atoms resulting in substantial increase in the I yield (up to 45 % related to HI (F_2)).
- Four different mixing/reacting schemes for the mutual reaction of F+HI+$O_2(^1\Delta_g)$, and I+$O_2(^1\Delta_g)$ were considered in the modeling.
- A subsonic mixing of F, HI and $O_2(^1\Delta_g)$, or I and $O_2(^1\Delta_g)$ near the nozzle entrance could provide a sufficient production of I^* for lasing.
- Generation of F or I atoms in a separate reactor, and their introduction into the primary $O_2(^1\Delta_g)$ flow in COIL seems to be the most advantageous procedure. Also a supersonic mixing of atomic iodine (generated separately) with $O_2(^1\Delta_g)$ gave acceptable results.

- Computational estimation of the quenching effect on I^* in this reaction system on the basis of known quenching rate constants was performed.
- Results of computational modeling are a good base for a design of experimental device.

4. Concluding note

Some of the results given in this report were recently presented at conferences and published in journals with the Acknowledgment to the USAF EOARD for the financial support. They are listed below:

O. Špalek, V. Jirásek, M. Censký, J. Kodymová, I. Jakubec
"Experimental results on chemical generation of atomic iodine"
COIL R&D Workshop, Prague, May, 2001.

V. Jirásek, O. Špalek, J. Kodymová, M. Censký
„Modeling of chemical generation of atomic iodine for a COIL"
COIL R&D Workshop, Prague, May, 2001.

V. Jirásek, O. Špalek, J. Kodymová, M. Censký
„*Chemical generation of atomic iodine for chemical oxygen-iodine laser: Modeling of reaction systems"*
Chemical Physics, **269,** 167 (2001).

J. Kodymová, O. Špalek
„A contribution of COIL Laboratory in Prague to the Chemical Oxygen-Iodine Laser research and development" (Invited talk)
Proc. Gas and Chemical Lasers and Intense Beam Applications III, San Jose, USA, SPIE Vol. **4631**, p. 86, 2002.

O. Špalek, V. Jirásek, J. Kodymová, M. Censký, I. Jakubec
„Chemical generation of atomic iodine for COIL"
Proc. Gas and Chemical Lasers and Intense Beam Applications III, San Jose, USA, SPIE Vol. **4631**, p. 34, 2002.

V. Jirásek, O. Špalek, J. Kodymová, M. Censký
„Modeling of the chemical generation of atomic iodine in a chemical oxygen-iodine laser"
Proc. Gas and Chemical Lasers and Intense Beam Applications III, San Jose, USA, SPIE Vol. **4631**, p. 43, 2002.

J. Kodymová, O. Špalek, V. Jirásek, M. Censký
„Review of chemical oxygen-iodine laser research in Prague COIL laboratory" (Invited talk)
Proc. Intern. Conference „Fourth Khariton's Topical Scientific Readings", Sarov, Russia, February, 2002.

O. Špalek, V. Jirásek, M. Censký, J. Kodymová, I. Jakubec, G.D. Hager
"Chemical generation of atomic iodine for the chemical-oxygen iodine laser: Experimental results"
Chemical Physics, accepted for publication, May 2002.

J. Kodymová, O. Špalek, V. Jirásek, M. Censký, G.D. Hager
"Recent results in the development of a chemical way of atomic iodine generation for a COIL"
Proc. Intern. Conference High-Power Laser Ablation, Taos, NM, USA, April, 2002
SPIE Vol. (in press).

5. References

1. R.F. Tate, B.S. Hunt, C.A. Helms, K.A. Truesdell and G.D. Hager, IEEE J. Quan. Electron. **31**, 1632 (1995).
2. V. Jirásek, O. Špalek, J. Kodymová, Proc. SPIE **4184,** 103 (2000).
3. NIST Chemistry Webbbook.
4. R. Svehla, NASA Technical Report, NASA-TR-R-132, 1962.
5. O. Špalek, V. Jirásek, J. Kodymová, I. Jakubec, M. Censký, Proc. SPIE **4184,** 111 (2000).
6. J. Paschkewitz, J. Shang, J. Miller, T. Madden, AIAA 2000-2574, 1 (2000).

6. Acknowledgement

The investigators are very grateful to the USAF EOARD for the financial support of this work, and to Dr. Alexander Glass, Program Manager, Lasers and Photonics at the EAORD, for his assistance in the matters concentring this contract.

We thank very much Dr. Gordon Hager from the US AFRL/DE, the contract supervisor, for his encouragement in our work, and beneficial discussions with him on the contract tasks.

We also appreciate very much any help and contribution of colleagues from the AFRL (Dr. Timothy Madden, Dr. Brian Anderson, Dr. Ralph Tate), and the representatives of the US AFRL/DE at the Kirtland AFB, NM.

Acknowledgement of Support: This material is based upon work supported by the European Office of Aerospace Research and Development, Air Force Office of Scientific Research, Air Force Laboratory, under contract F61775-01-WE057.

Disclaimer: Any opinions, findings and conclusions or recommendations expressed in this material are those of the authors and do not necessarily reflect the views of the European Office of Aerospace Research and Development, Air Force Office of Scientific Research, Air Force Laboratory.

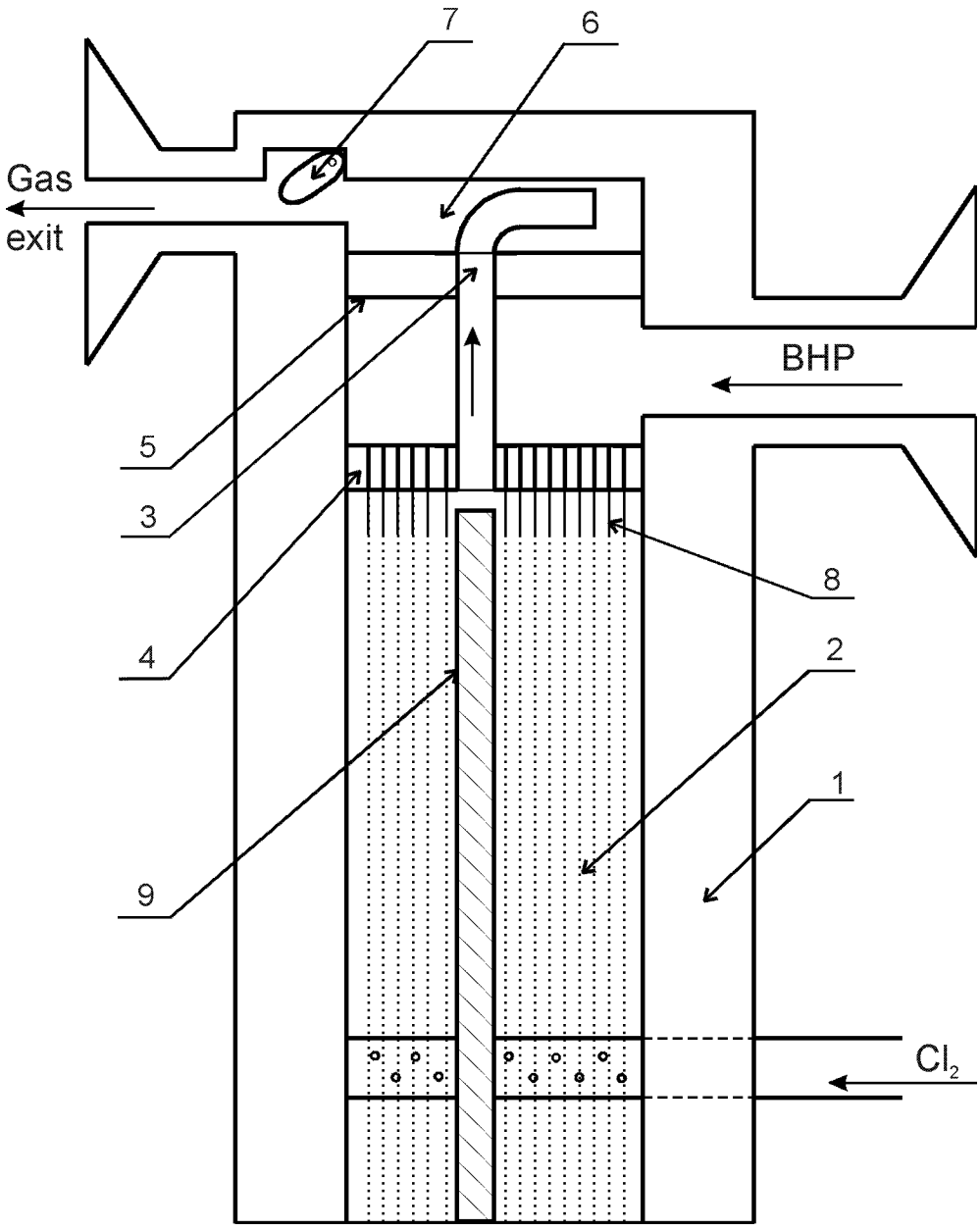

Fig. 1. Scheme of the jet SOG with vertical gas exit (arrows)

1 – generator body, 2 – g/l reactor, 3 – gas exit channel made of metal tubes bent in upper part opposite to gas flow,
4 – BHP injector, 5 – plate dividing BHP cavity and gas space,
6 – gas space, 7 – throttle valve, 8 – needles, 9 – plastic plate

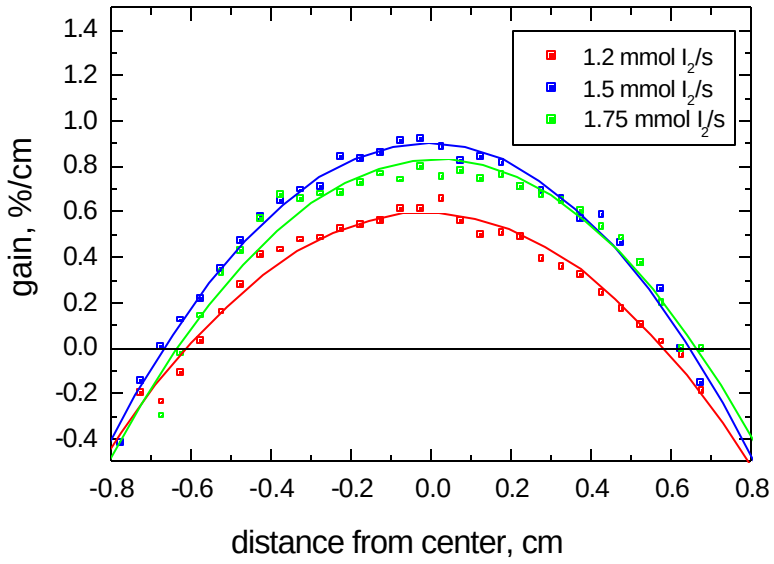

Fig. 2. Gain distribution in vertical direction, 5.5 cm downstream from nozzle throat at different iodine flow rate, 80 mmol He_{sec} s^{-1}

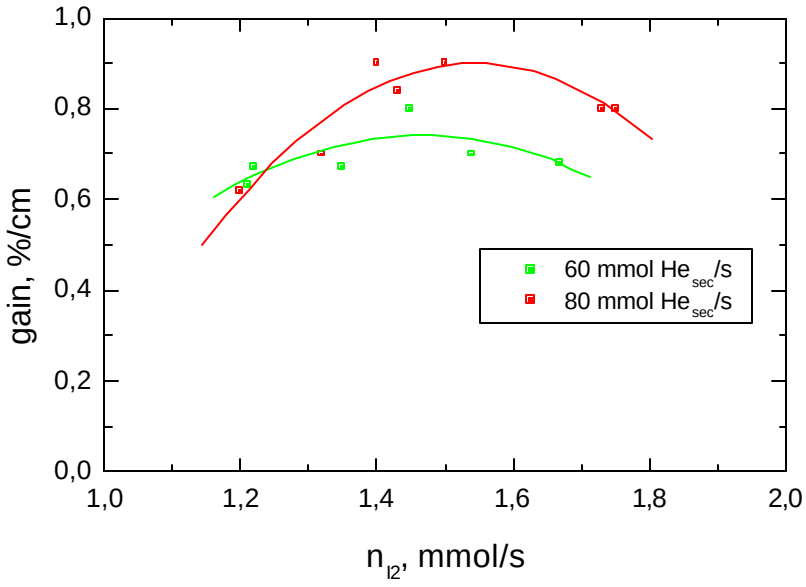

Fig. 3. Dependence of gain in cavity center on iodine flow rate at distance 5.5 cm from nozzle throat, flow rate of secondary helium 60 and 80 mmol s^{-1}

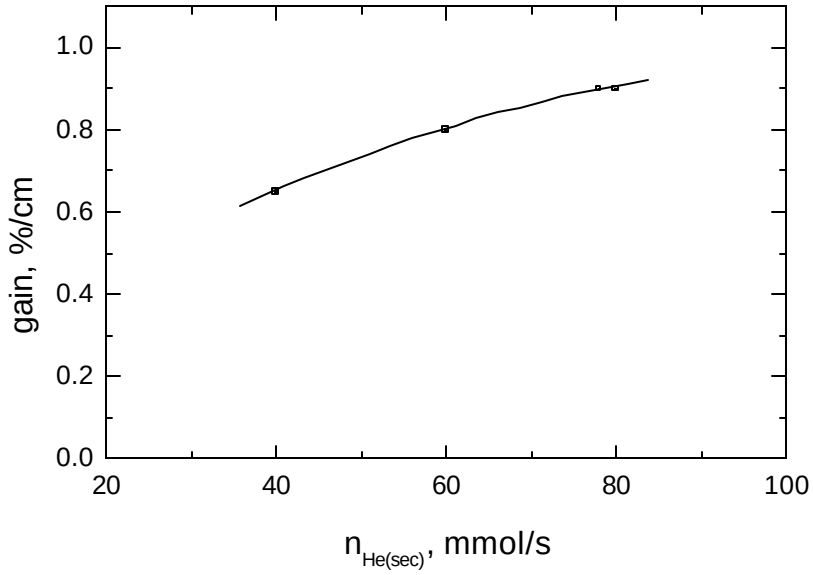

Fig. 4. Dependence of gain in cavity center on secondary helium flow rate at distance 5.5 cm from nozzle throat, 1.5 mmol I_2 s^{-1}

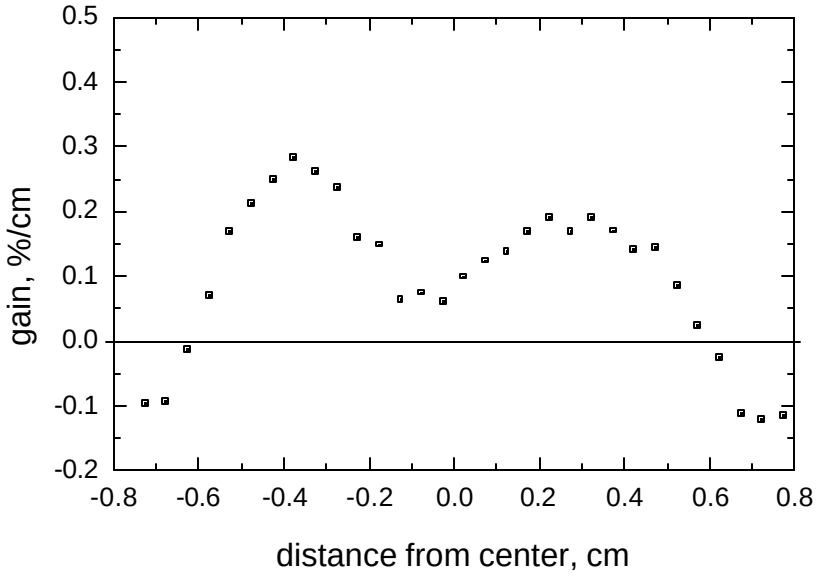

Fig. 5. Gain distribution in vertical direction, 5.5 cm downstream from the nozzle throat, 1.5 mmol I_2 s^{-1}, 40 mmol He_{sec} s^{-1}

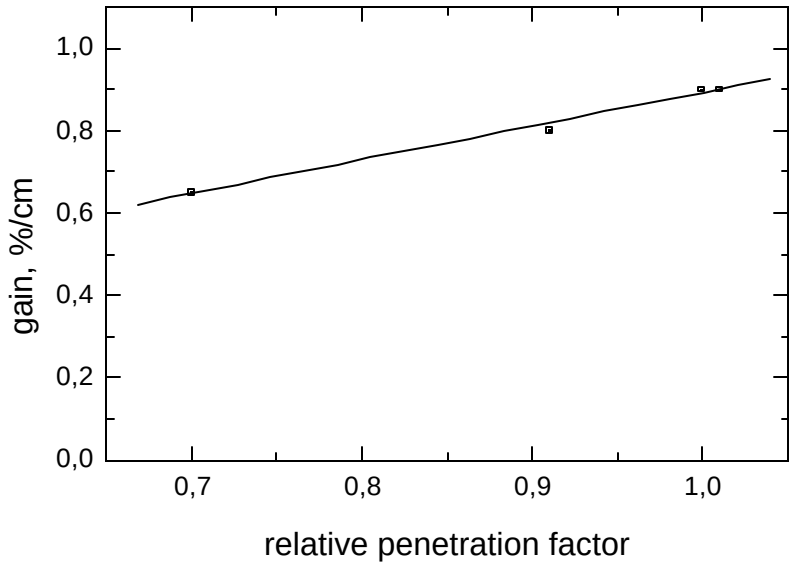

Fig. 6. Dependence of gain in cavity center on relative penetration factor at distance 5.5 cm from nozzle throat, 1.5 mmol I_2 s^{-1}

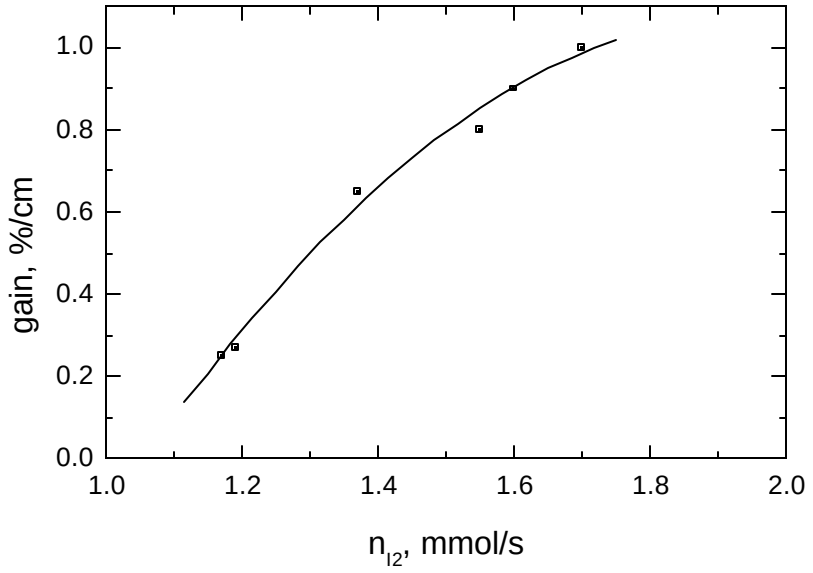

Fig. 7. Dependence of gain in cavity center on iodine flow rate at distance 4.1 cm from nozzle throat, 80 mmol He_{sec} s^{-1}

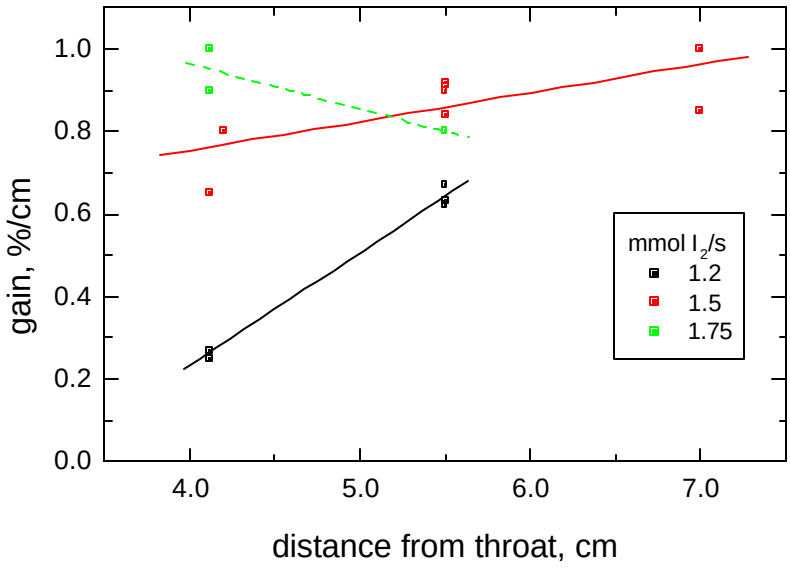

Fig. 8. Dependence of gain in cavity center on distance from nozzle throat, and at different iodine flow rate, 80 mmol He_{sec} s^{-1}

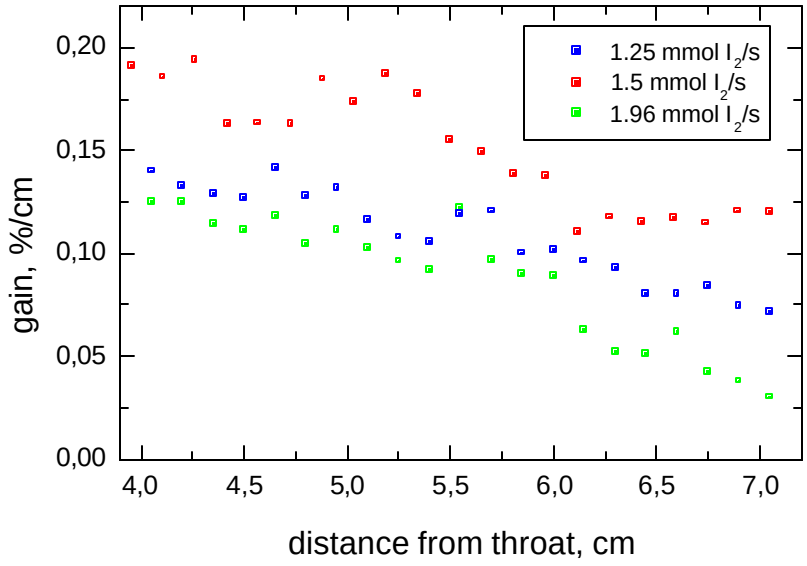

Fig. 9. Gain distribution in cavity center in horizontal direction, at different iodine flow rate, 40 mmol He_{sec} s^{-1}

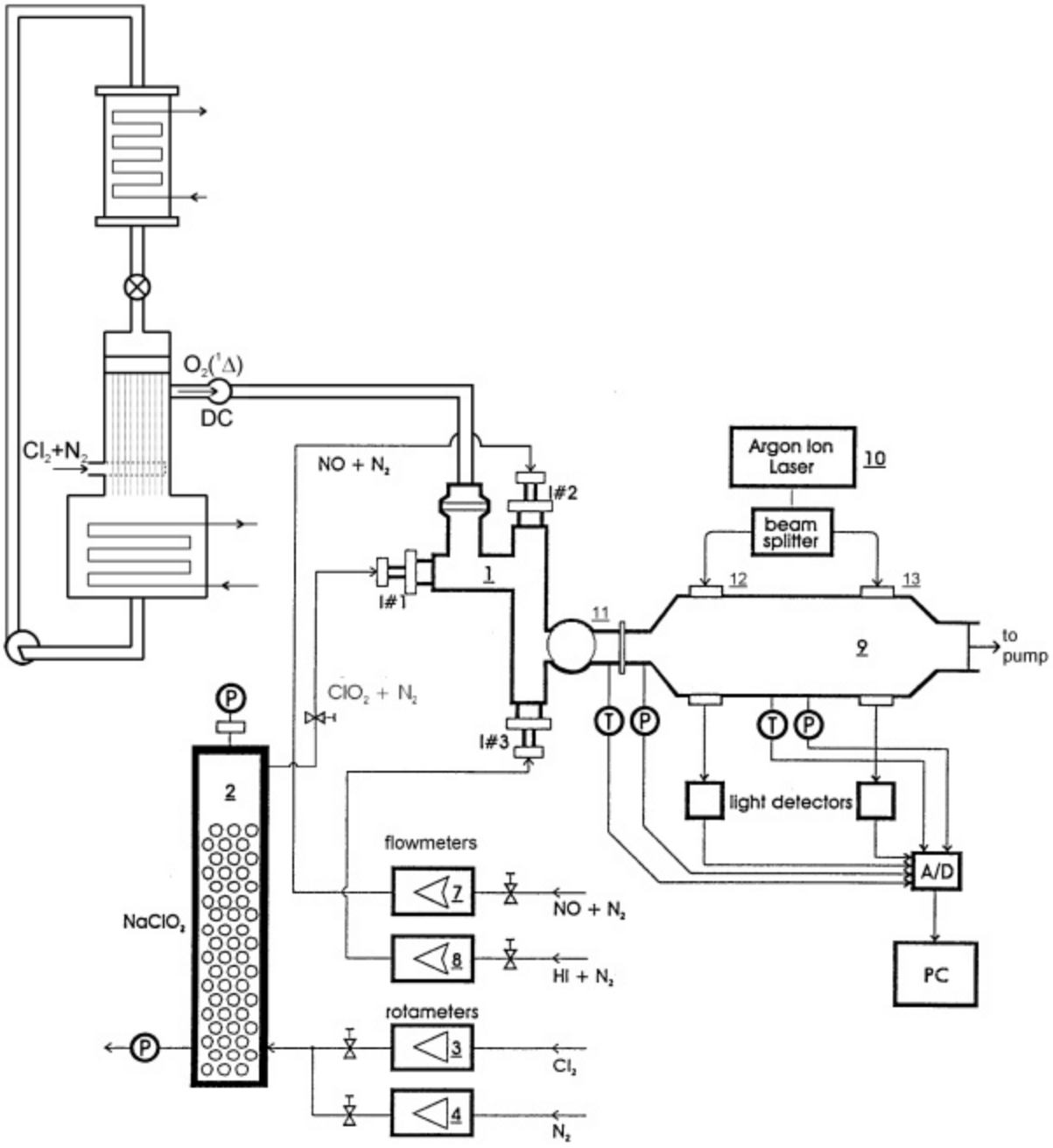

Fig. 10. Schematic small-scale device for chemical generation of atomic iodine in flow of singlet oxygen generated in jet SOG.
1 – reactor for I atoms generation; 2 – generator of ClO_2;
3,4 – gas management with rotameters; 7,8 – flowmeters; I #1-3 injectors for ClO_2, NO, and HI; 9 – detection flow cell for I_2;
10 – Ar ion laser; 12,13 – optical cells for I_2 detection by Ar ion laser beam.

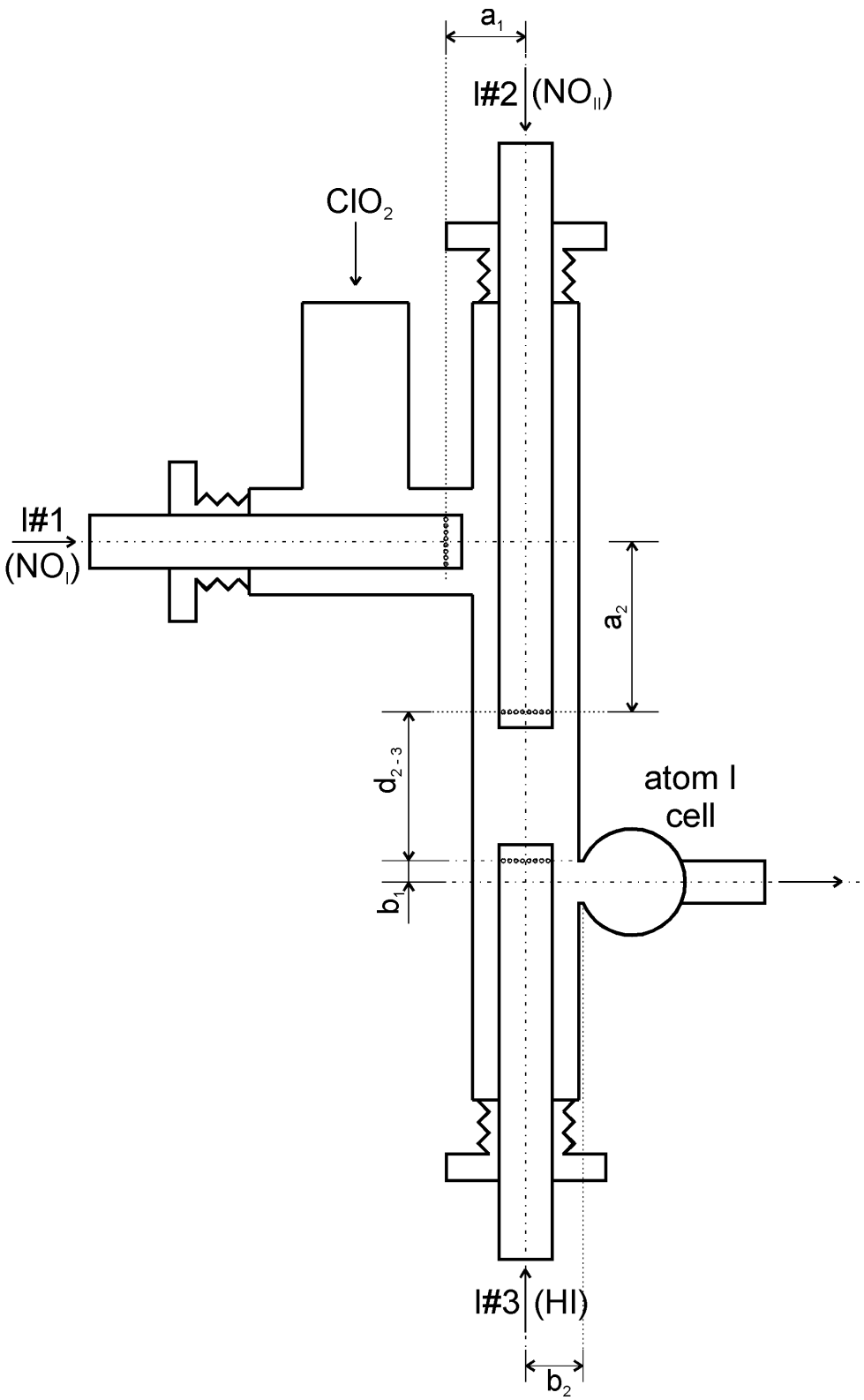

Fig. 11. Cross section of I atom reactor

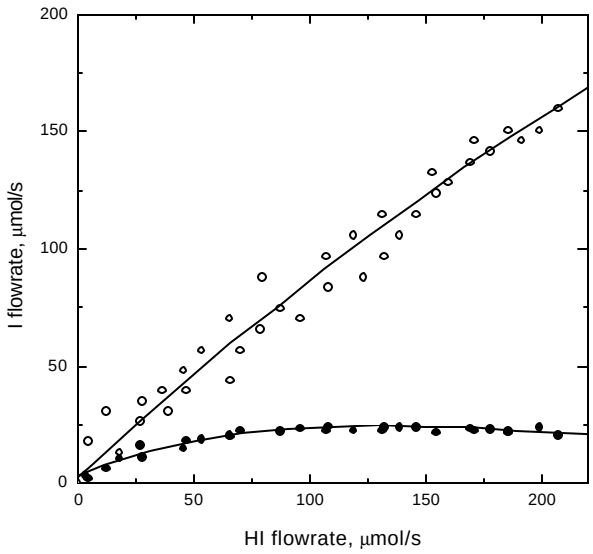

Fig. 12. Overall rate of atomic iodine production (o), and the rate estimated by the ISD (•) and its dependence on HI flow rate; primary flow: 220 μmol ClO_2 s^{-1} + 2 mmol N_2 s^{-1}, 2nd injector: 375 μmol NO s^{-1}, 3rd injector: HI; total pressure 2–2.9 kPa; distance between injectors: $d_{2\text{-}3}$ = 3.7 mm, and 3rd injector - ISD cell: $d_{3\text{-ISD}}$ = 11 mm.

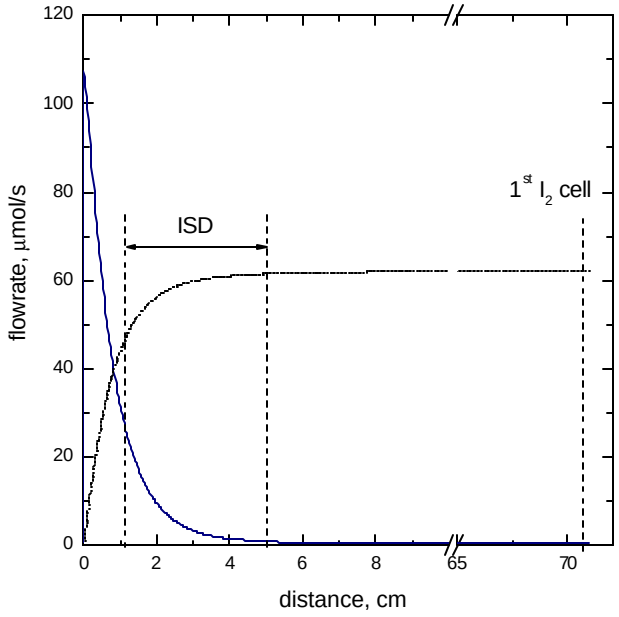

Fig. 13. Calculated time development I and I_2 flow rates downstream from the 3rd injector 220 μmol HI s^{-1}, gas velocity 85 m s^{-1}, and other conditions as in Fig.12.

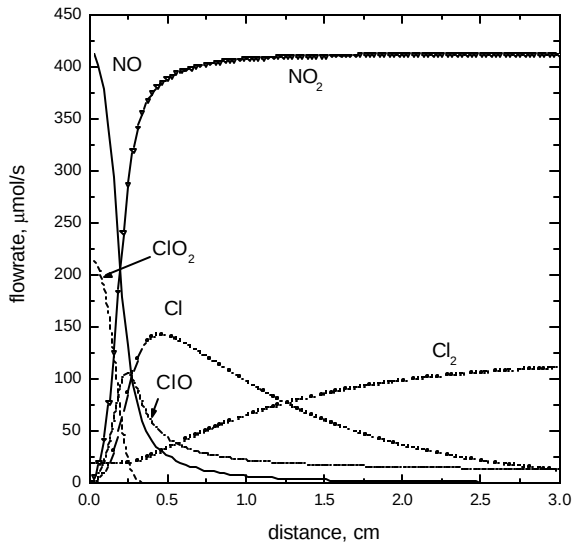

Fig. 14. Time history of reactants and reaction products downstream from NO injector calculated for 220 µmol ClO_2 s^{-1} + 2 mmol N_2 s^{-1} in primary flow, 420 µmol NO s^{-1}; gas velocity 140 m s^{-1}, and total pressure 2.3 kPa

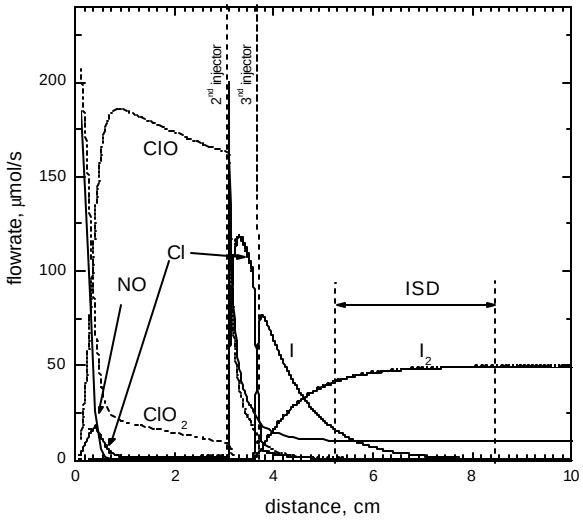

Fig. 15. Time history of reactants and reaction products and I atom production calculated for 220 µmol ClO_2 s^{-1} + 2 mmol N_2 s^{-1} in primary flow, 200 µmol NO s^{-1}
(1^{st} inj.), 200 µmol NO s^{-1} (2^{nd} inj.), 100 µmol HI s^{-1} (3^{rd} inj.); total pressure 2.7 kPa; d_{1-2} = 30 mm, and d_{2-3} = 3.7 mm; gas velocity between 1^{st} and 3^{rd} injector: 140 m s^{-1}, downstream 3^{rd} injector: 85 m s^{-1}.

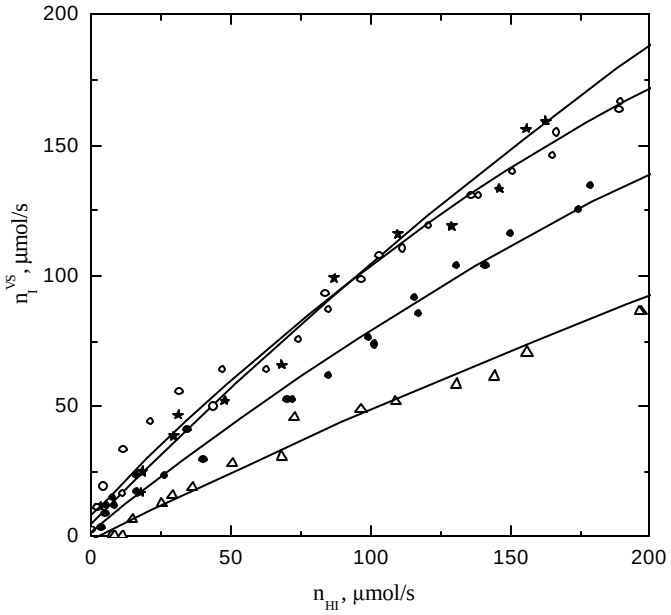

Fig. 16. Dependence of the overall flow rate of atomic iodine (measured in cell 12) on HI flow rate at 220 µmol ClO_2 s^{-1}, and various NO flow rate: 205 µmol s^{-1} (ξ), 330 µmol s^{-1} (o), 440 µmol s^{-1} (•), 560 µmol s^{-1} (Δ); for other conditions see Fig. 12.

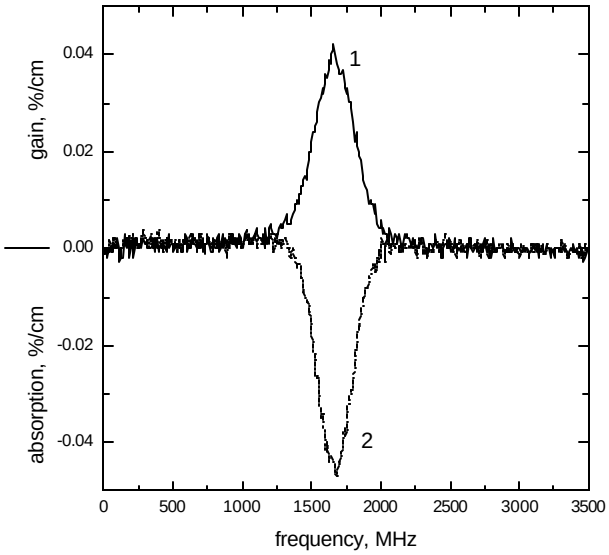

Fig. 17. Absorption/emission (gain) curve for atomic iodine recorded for primary flow of either 30 µmol ClO_2 s^{-1}+2.5 mmol N_2 s^{-1} (curve 2), or 30 µmol ClO_2 s^{-1}+2.5 mmol N_2 s^{-1}+0.9 mmol $O_2(^1\Delta_g)$ s^{-1}+1.4 mmol $O_2(^3\Sigma_g)$ s^{-1}(curve 1); 225 µmol NO s^{-1} (2^{nd} inj.), 30 µmol HI s^{-1} (3^{rd} inj.); $d_{2\text{-}3}$ = 3.7 mm, $d_{3\text{-}ISD}$ = 11 mm; total pressure 1.8 kPa.

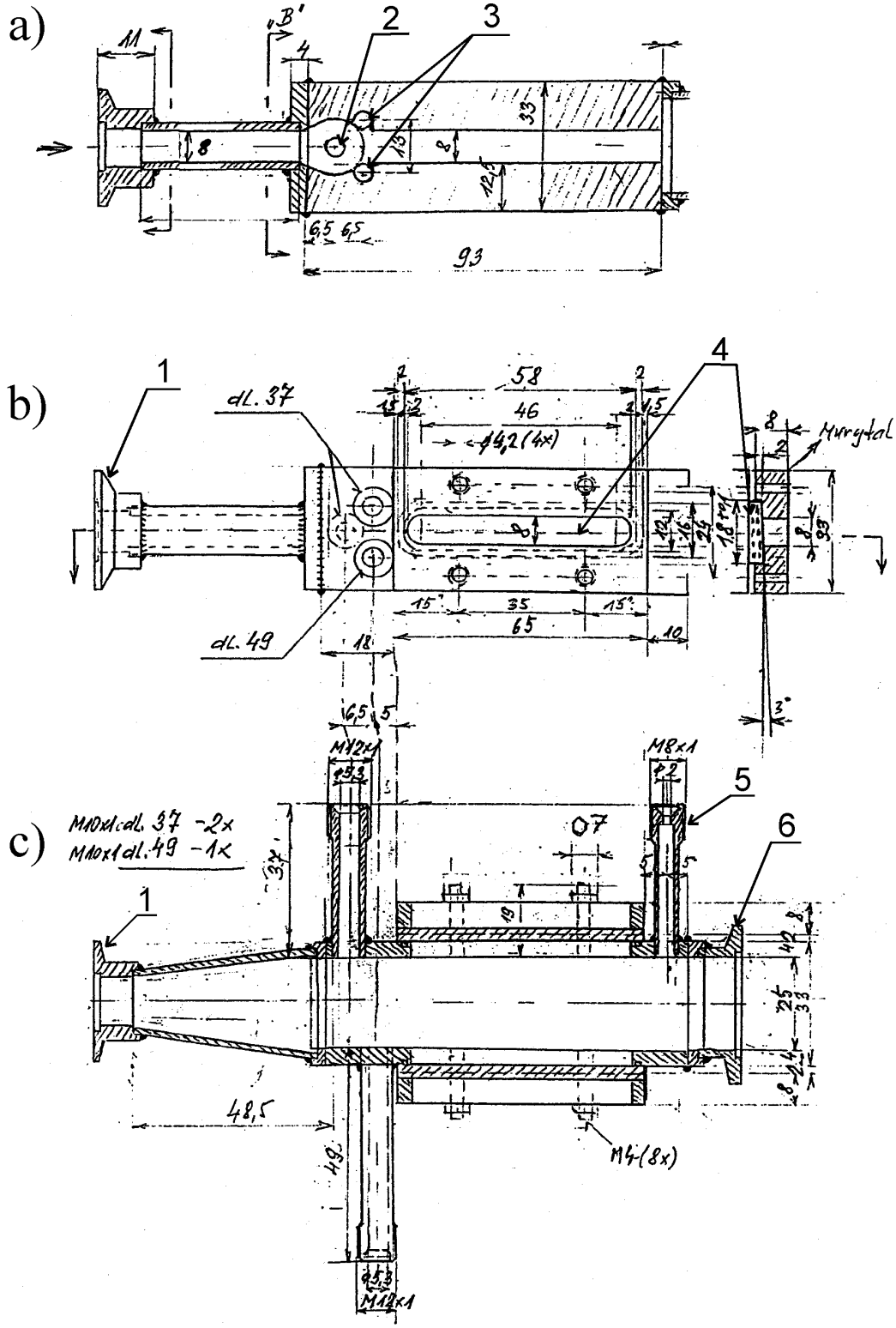

Fig. 18. Vertical cross-section (a), side view (b), and horizontal cross-section (c) of reactor with the probe beam perpendicular to gas flow direction.

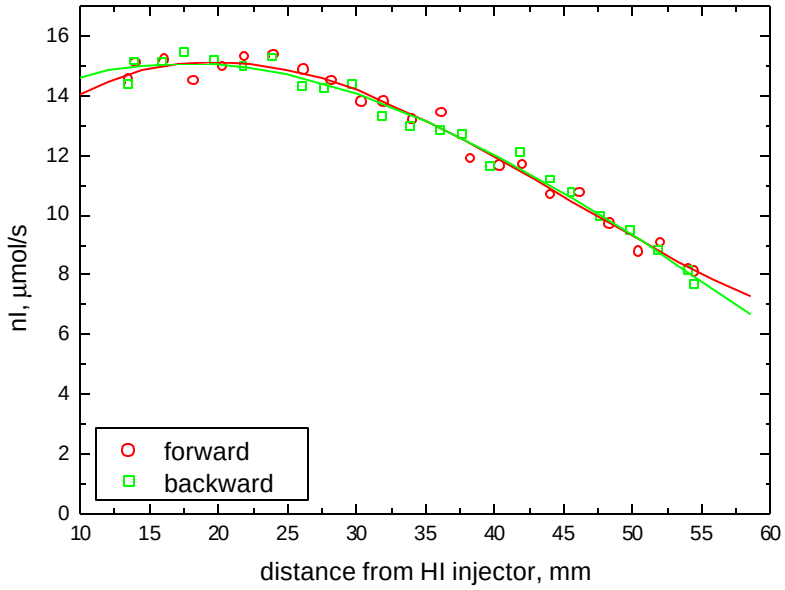

Fig. 19. Flow rate of atomic iodine in dependence on distance from HI injector. 57 µmol ClO_2 s^{-1} + 120 µmol NO s^{-1} + 50 µmol HI s^{-1}, T = 350 K, p = 1 kPa, d_{NO-HI} = 7 mm, v = 40 m s^{-1}

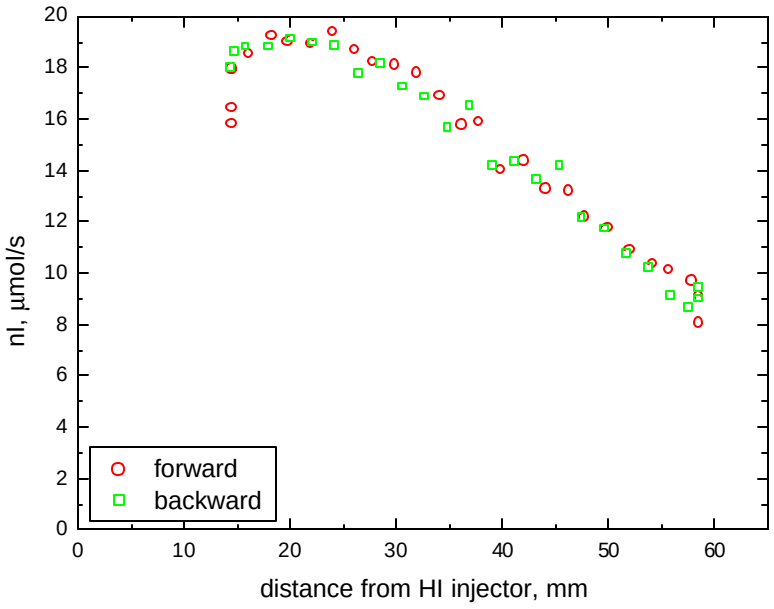

Fig. 20. Flow rate of atomic iodine in dependence on distance from HI injector. 33 µmol ClO_2 s^{-1} + 90 µmol NO s^{-1} + 42 µmol HI s^{-1}, p = 1 kPa, d_{NO-HI} = 7 mm, v = 40 m s^{-1}

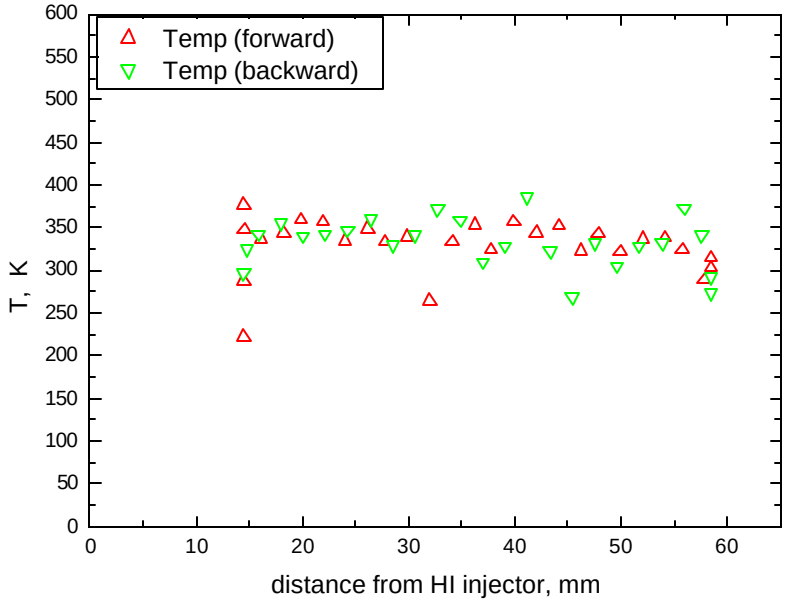

Fig. 21. Gas temperature in dependence on distance from HI injector. 33 µmol ClO_2 s^{-1} + 90 µmol NO s^{-1} + 42 µmol HI s^{-1}, p = 1 kPa, d_{NO-HI} = 7 mm, v = 40 m s^{-1}

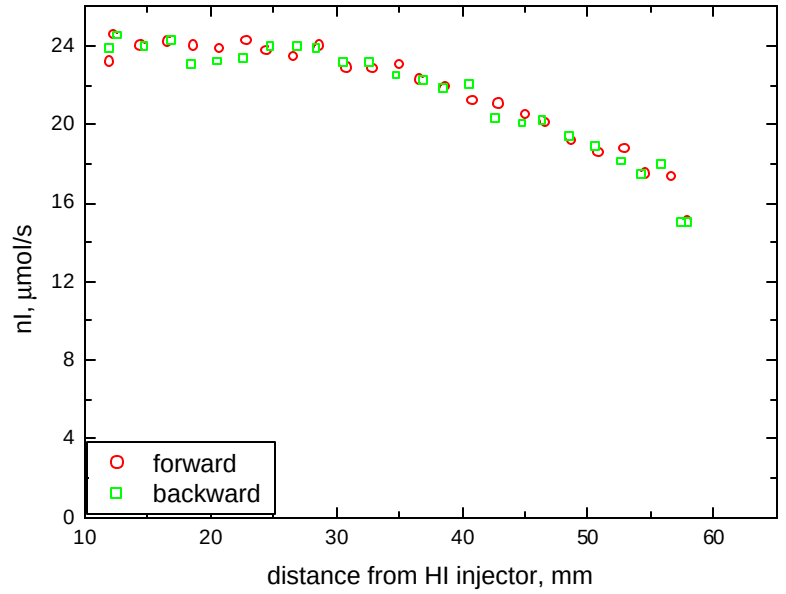

Fig. 22. Flow rate of atomic iodine in dependence on distance from HI injector. 73 µmol ClO_2 s^{-1} + 157 µmol NO s^{-1} + 67 µmol HI s^{-1}, T = 380 K, p = 1.2 kPa, d_{NO-HI} = 0 mm, v = 40 m s^{-1}

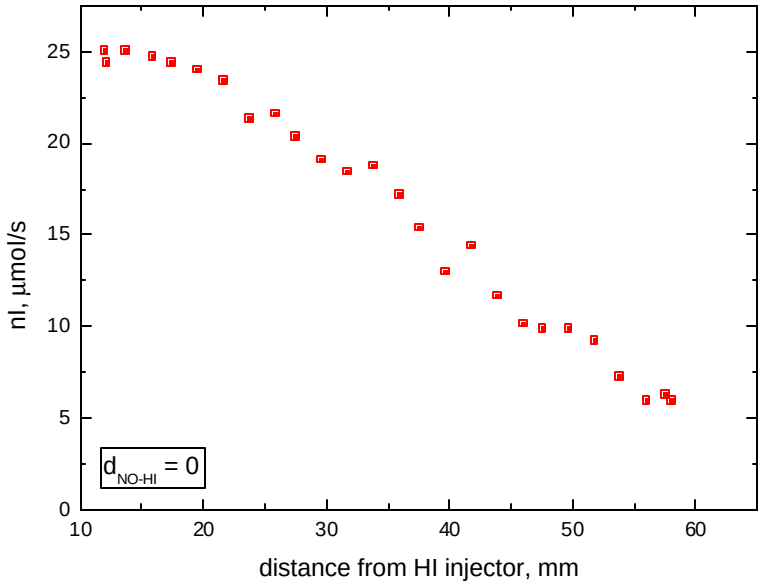

Fig. 23. Flow rate of atomic iodine in dependence on distance from HI injector. 134 µmol ClO_2 s^{-1} + 274 µmol NO s^{-1} + 208 µmol HI s^{-1}, T = 390 K, p = 2.55 kPa, d_{NO-HI} = 0 mm, v = 40 m s^{-1}

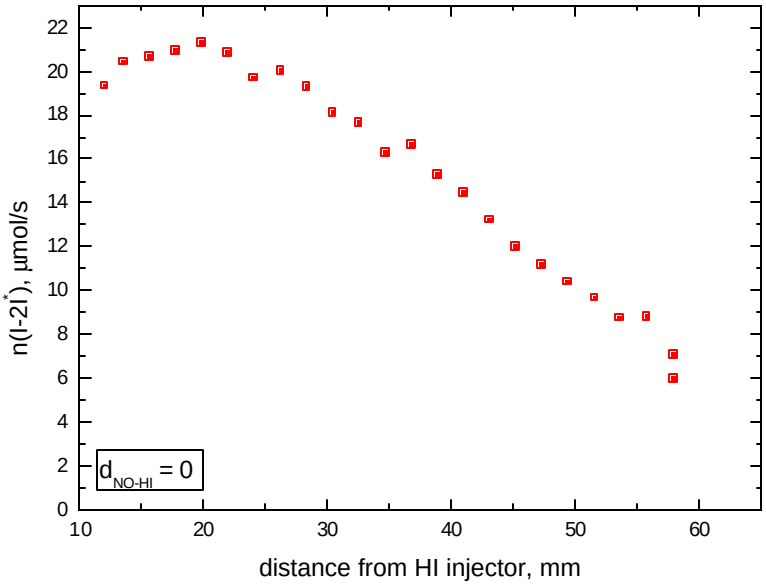

Fig. 24. Flow rate of atomic iodine in dependence on distance from HI injector. 24 µmol ClO_2 s^{-1} + 60 µmol NO s^{-1} + 40 µmol HI s^{-1}, T = 340 K, p = 1 kPa, d_{NO-HI} = 0 mm, v = 40 m s^{-1}

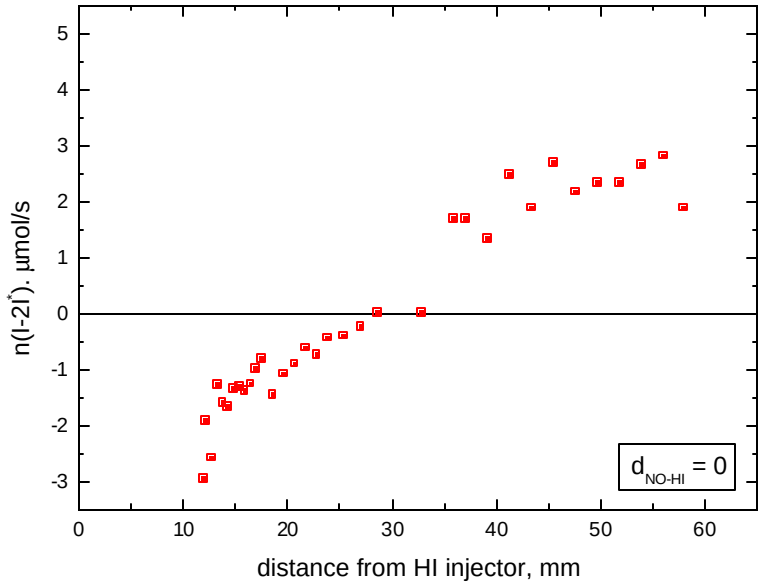

Fig. 25. Dependence of $n_{I-I^{*}/2}$ on distance from HI injector in $O_2(^1?)$ flow. 24 µmol ClO_2 s^{-1} + 60 µmol NO s^{-1} + 25 HI, $n_{O_2(^1\Delta)}$ = 560 µmol s^{-1}, p = 1.35 kPa, T = 400–450 K

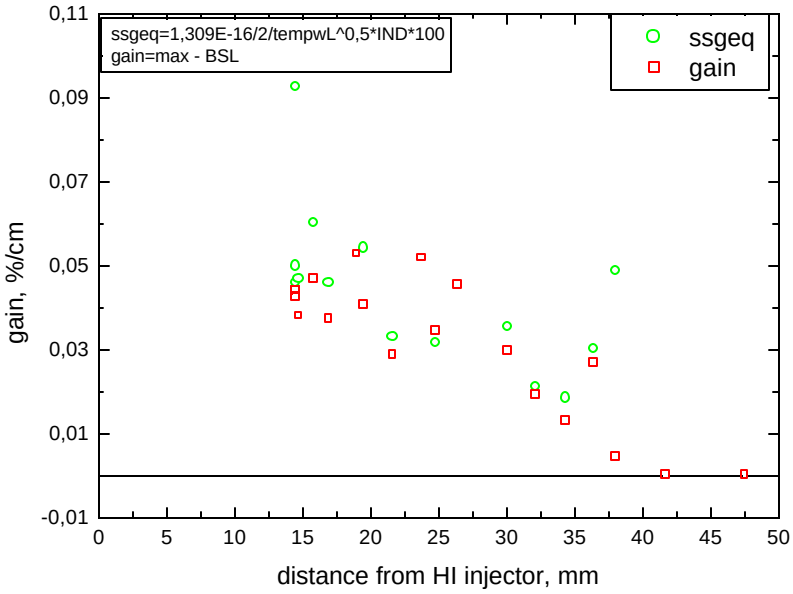

Fig. 26. Dependence of gain on distance from HI injector in $O_2(^1?)$ flow. 26 µmol ClO_2 s^{-1} + 54 µmol NO s^{-1} + 24 HI + 650 µmol $O_2(^1?)$ s^{-1}, p = 1.5 kPa, T = 430 K

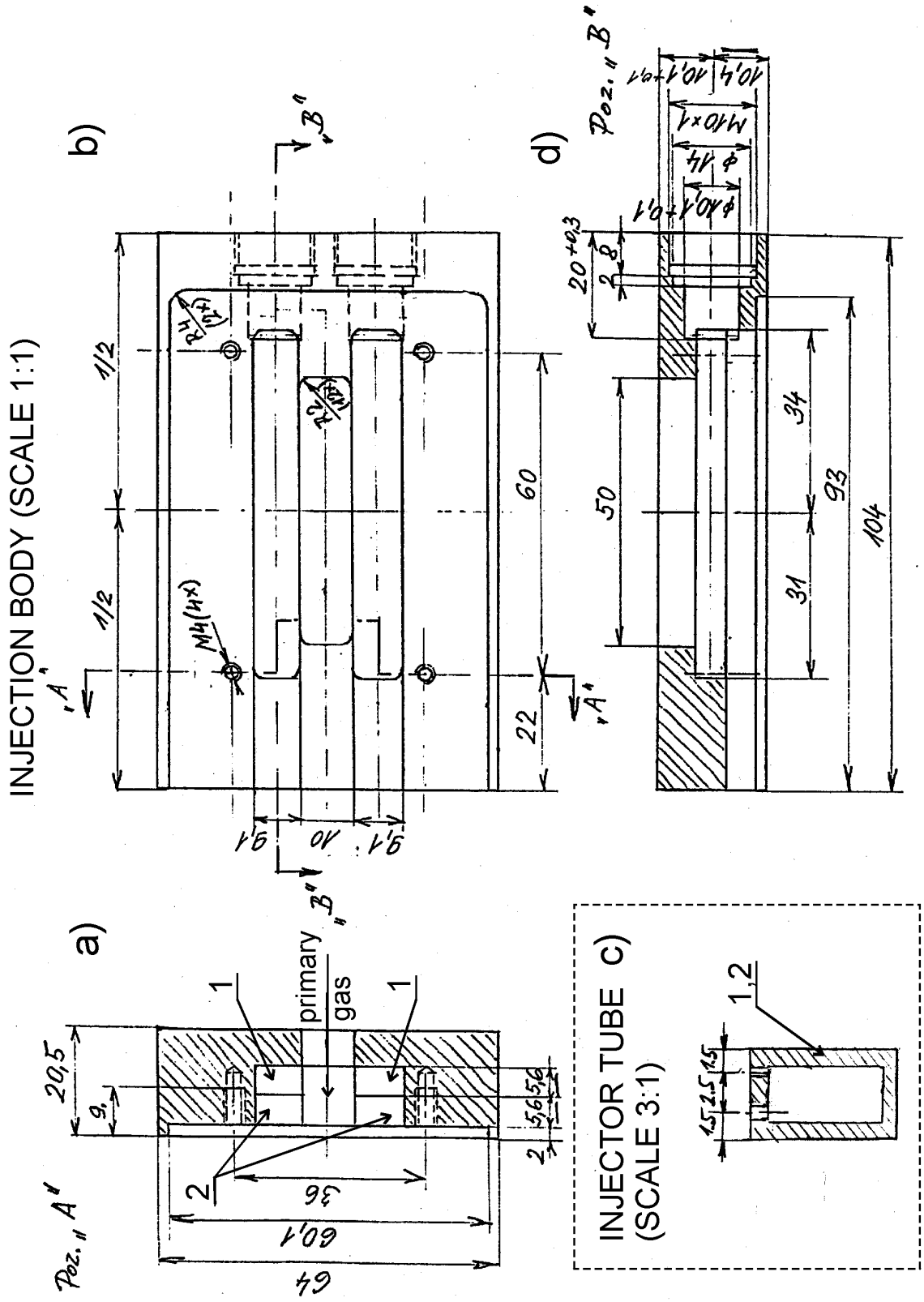

Fig. 27. Vertical cross-section (a), vertical view (b), and horizontal cross-section (c) of injector body, and vertical cross-section of injector tube (d).

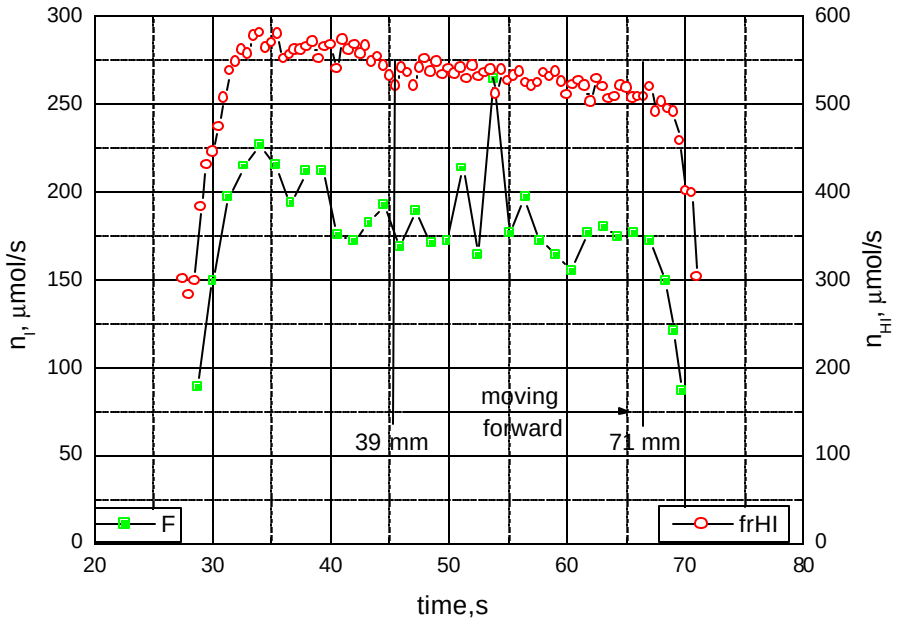

Fig. 28. Time course of atomic iodine flow rate and HI flow rate. 0.46 mmol ClO_2 s^{-1} + 2.1 mmol NO s^{-1} , p_{sub} 1.4 kPa, p_{cav} = 190 Pa, T_{cav} = 267 K, M = 1.7

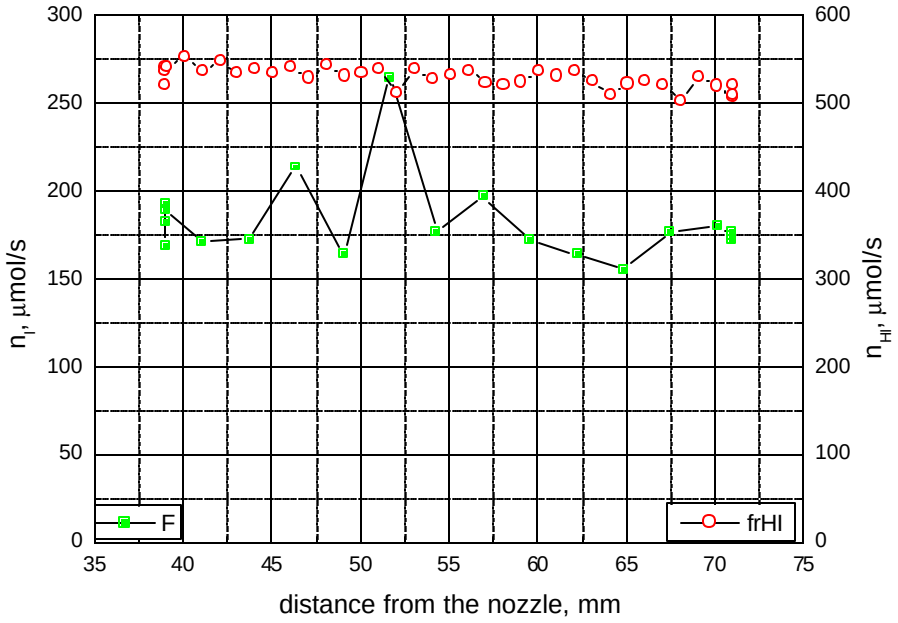

Fig. 29. Atomic iodine flow rate in dependence on distance from the nozzle plane. Other data as in Fig. 28

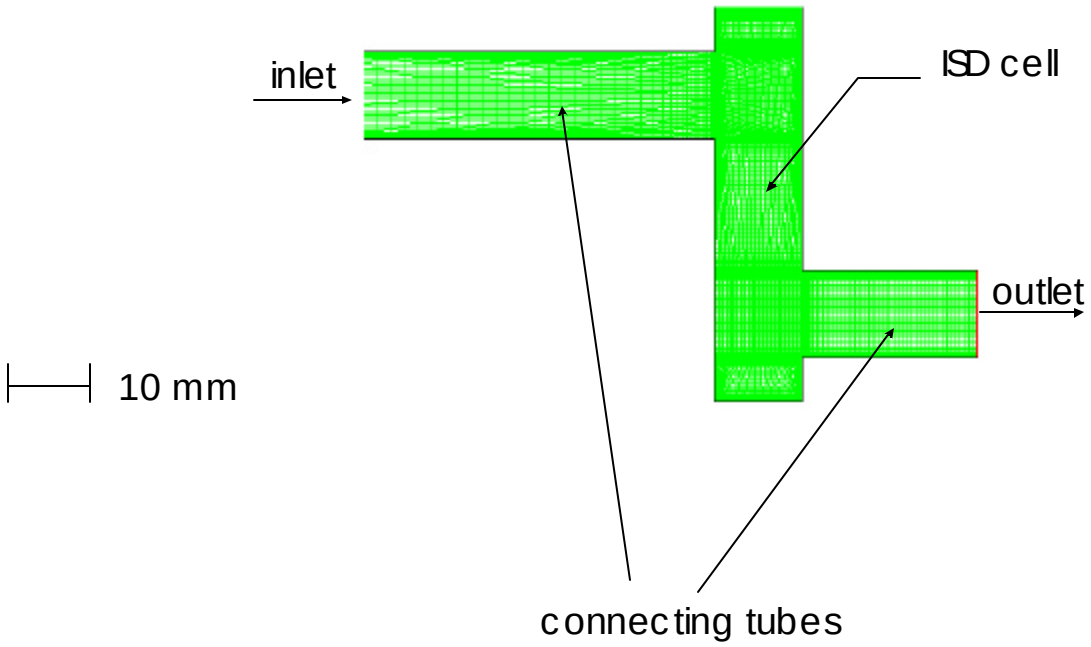

Fig. 30. Schematic diagram of ISD cell and computational mesh

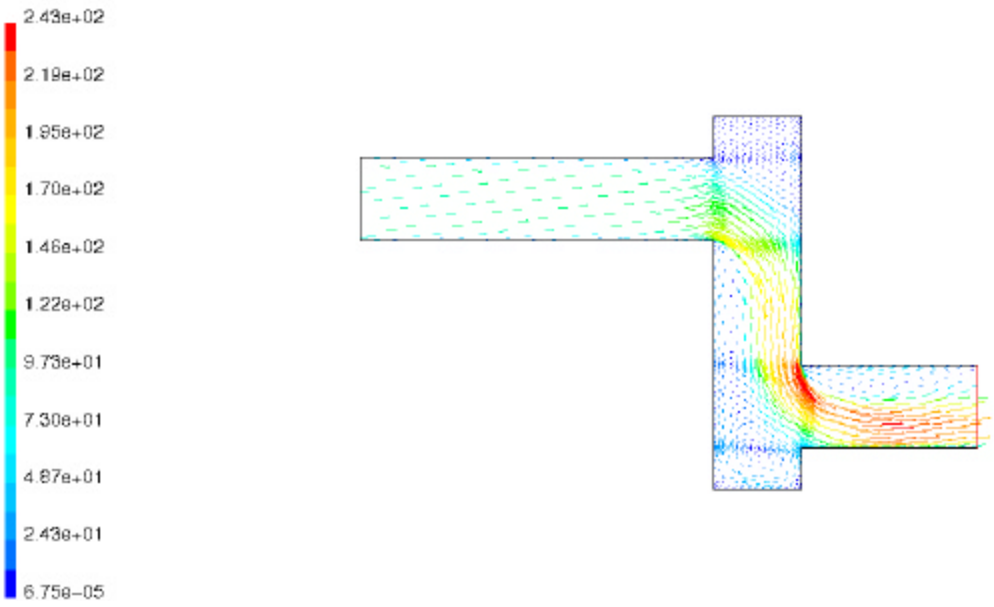

Fig. 31. Velocity vectors colored by velocity magnitude for ISD cell

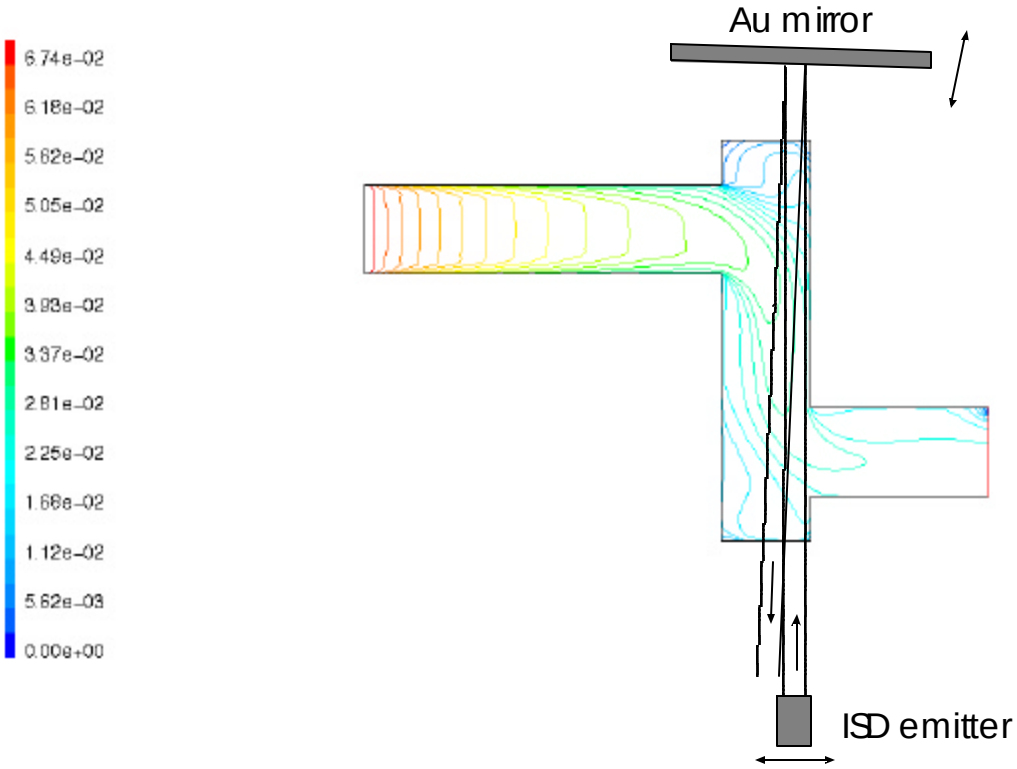

Fig. 32. Atomic iodine mass fraction and position of the laser probe beam

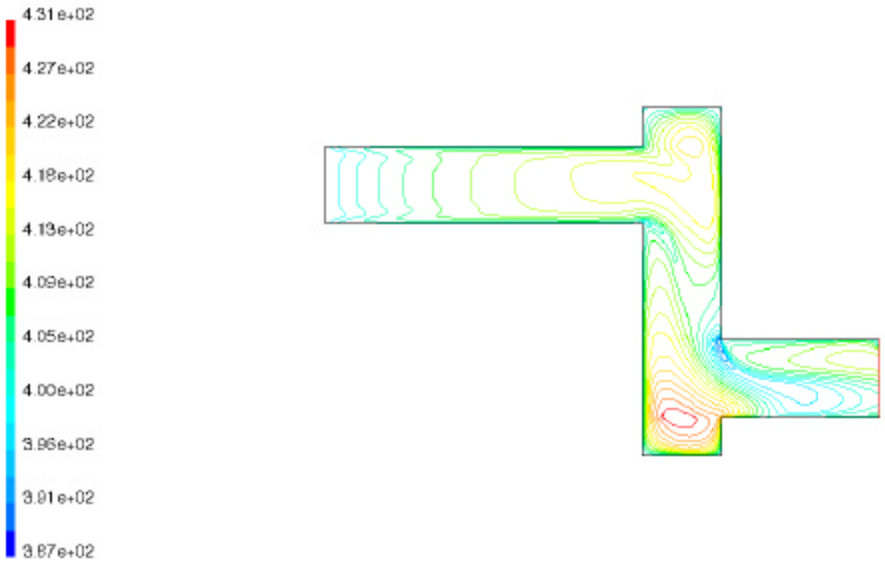

Fig. 33. Contours of static temperature (K) in ISD cell

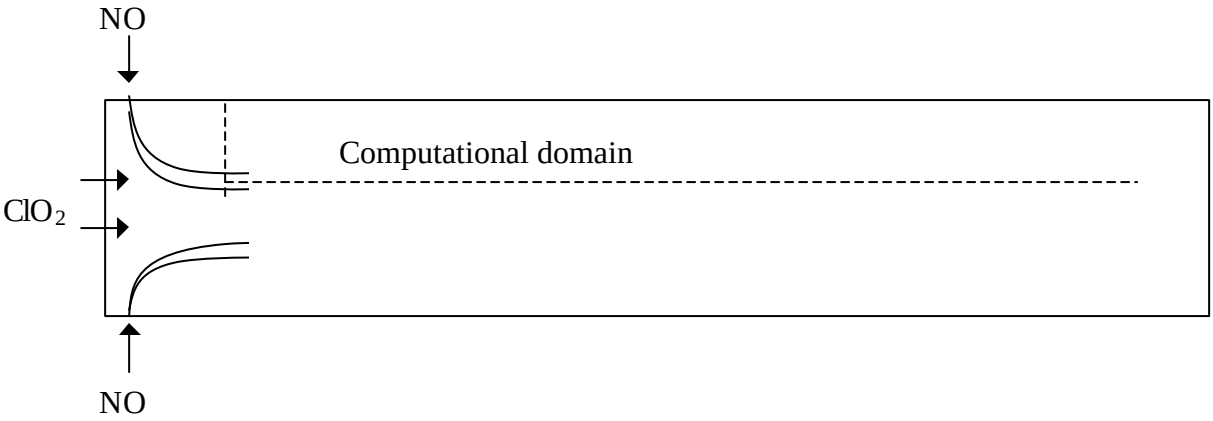

Fig. 34. Schematic diagram for NO and ClO_2 mixing

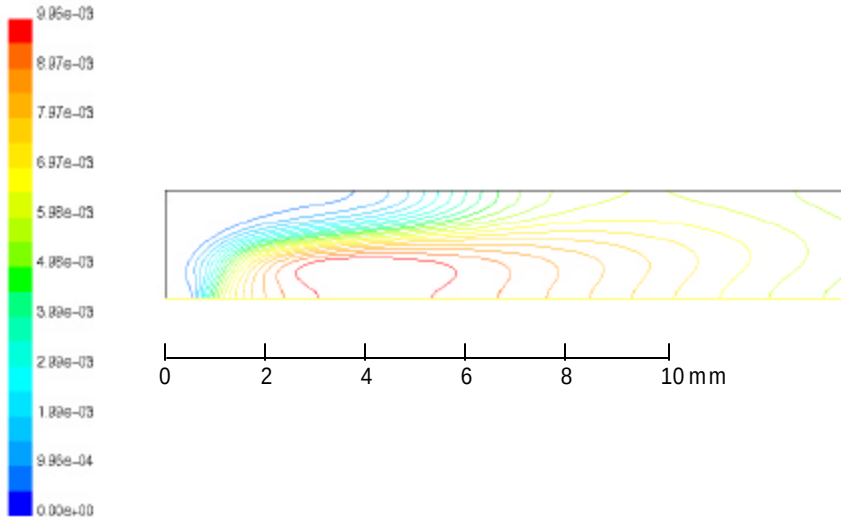

Fig. 35 a. Contours of mass fraction of Cl atoms for the ratio NO:ClO2 = 1:1

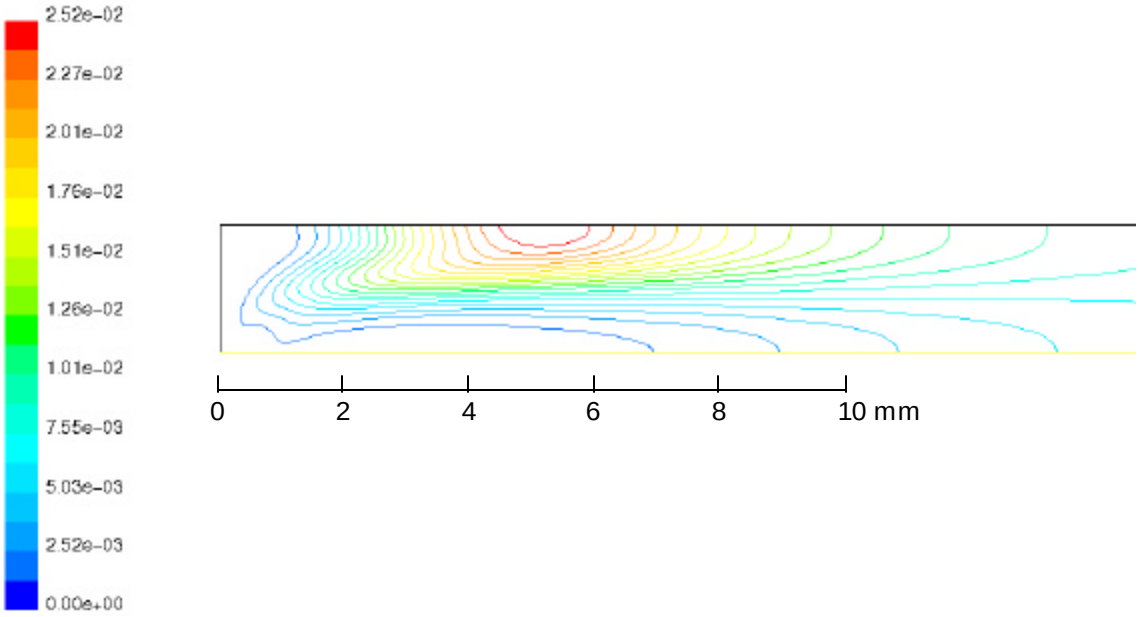

Fig. 35 b. Contours of mass fraction of ClO for the ratio $NO:ClO_2 = 1:1$

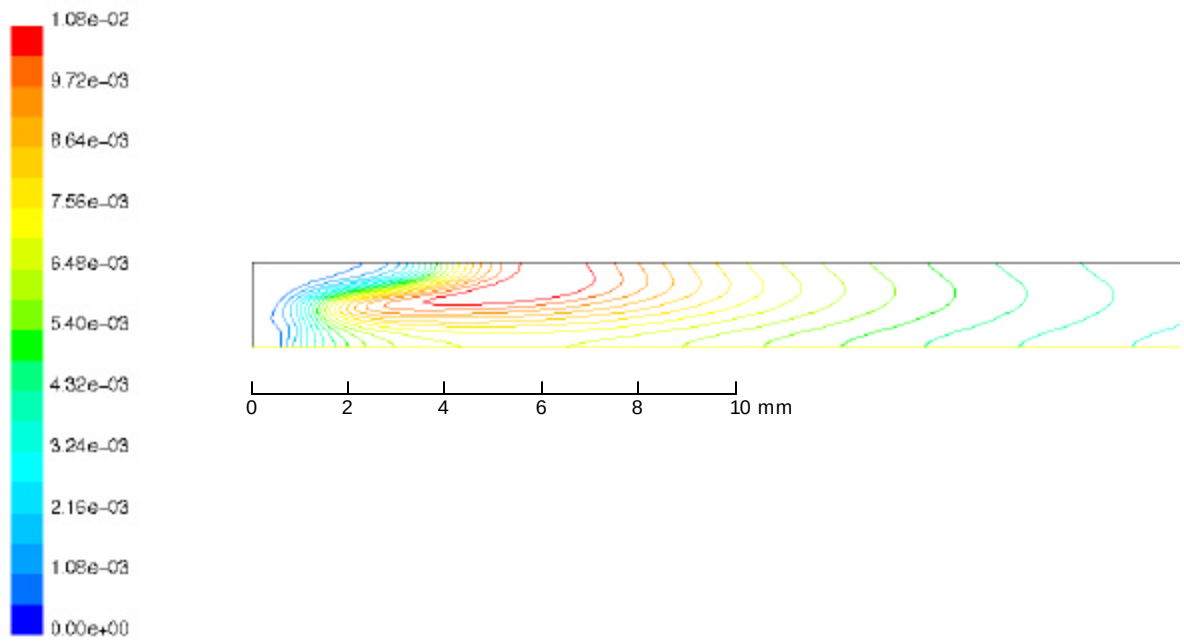

Fig. 36 a. Contours of mass fraction of Cl atoms for the ratio NO:ClO_2 = 2:1

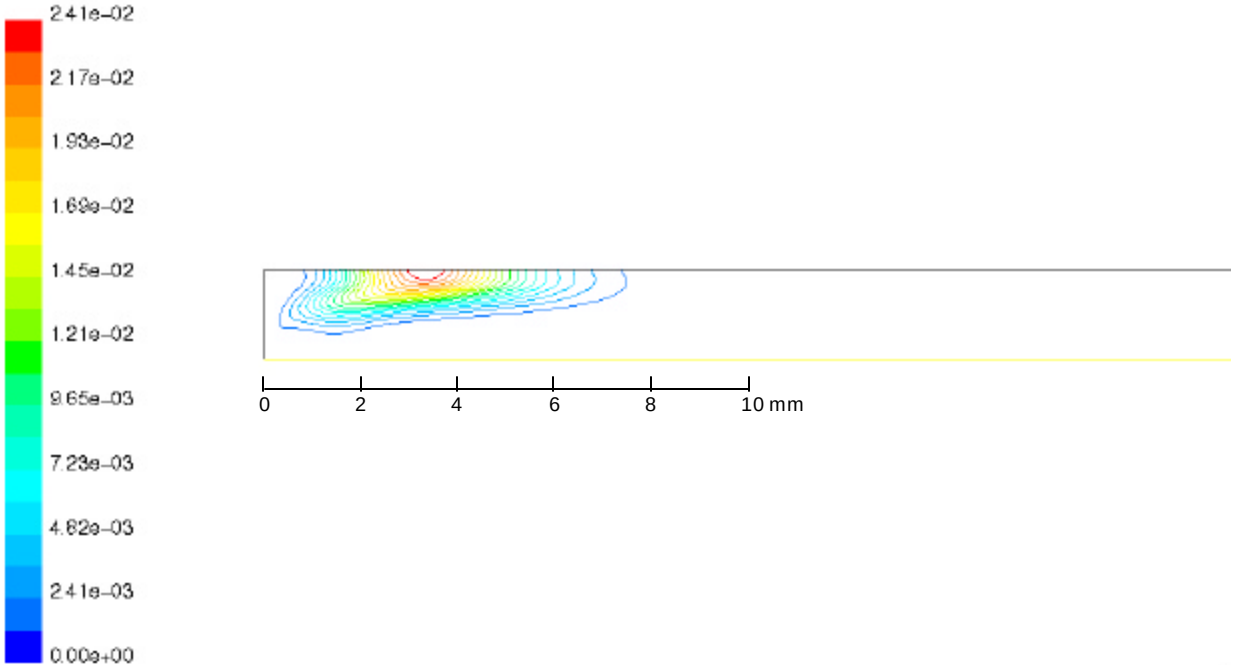

Fig. 36 b. Contours of mass fraction of ClO for the ratio NO:ClO_2 = 2:1

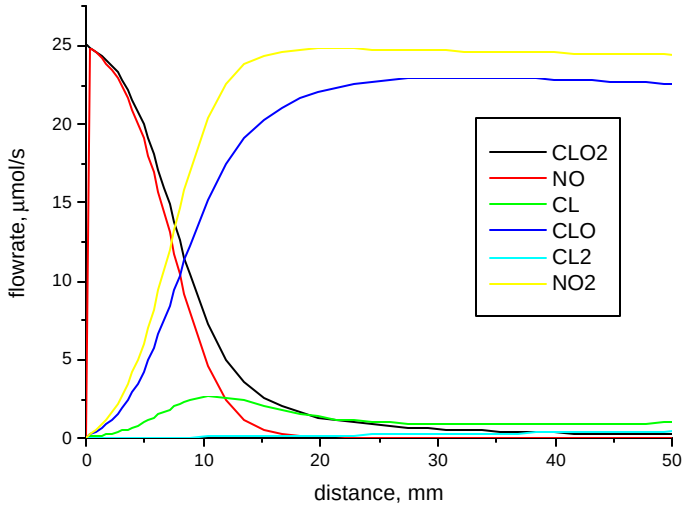

Fig. 37. Flow rates of main reactants and products calculated by 1-D model for the ratio NO:ClO_2 = 1:1

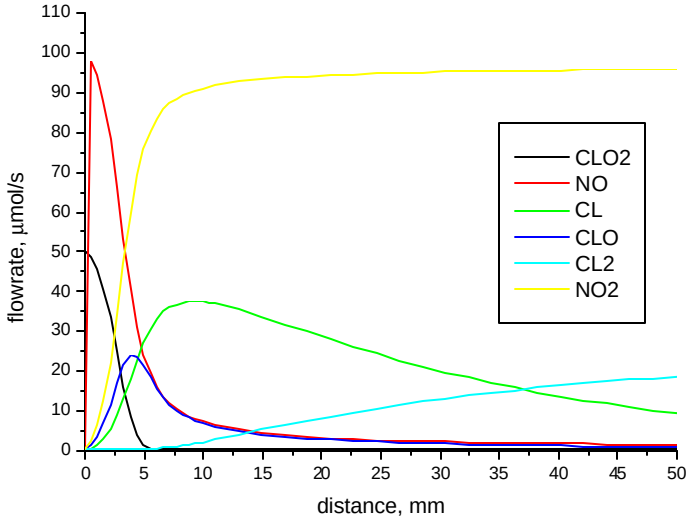

Fig. 38. Flow rates of main reactants and products calculated by 1-D model for the ratio NO:ClO_2 = 2:1

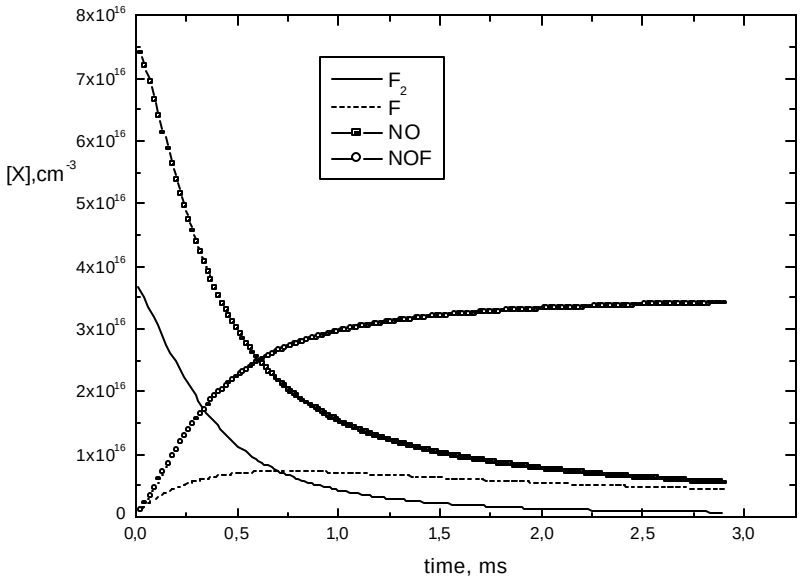

Fig. 39. Fluorine atoms production. Time development of concentration of different species [X] in reaction system. Initial concentration ratio of $[F_2]$:[NO]:[He] =
1:2:23; initial pressure 4 kPa; T = 300 K

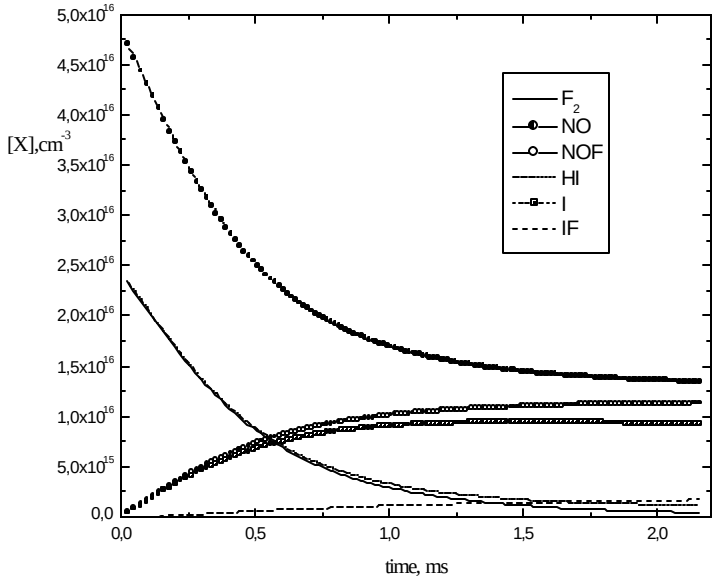

Fig. 40. Iodine atoms production. Time development of concentration of different species [X] in reaction system. Initial concentration ratio of $[F_2]$:[NO]:[HI]:[He] = 1:2:1:36; initial pressure 4 kPa; T = 300 K.

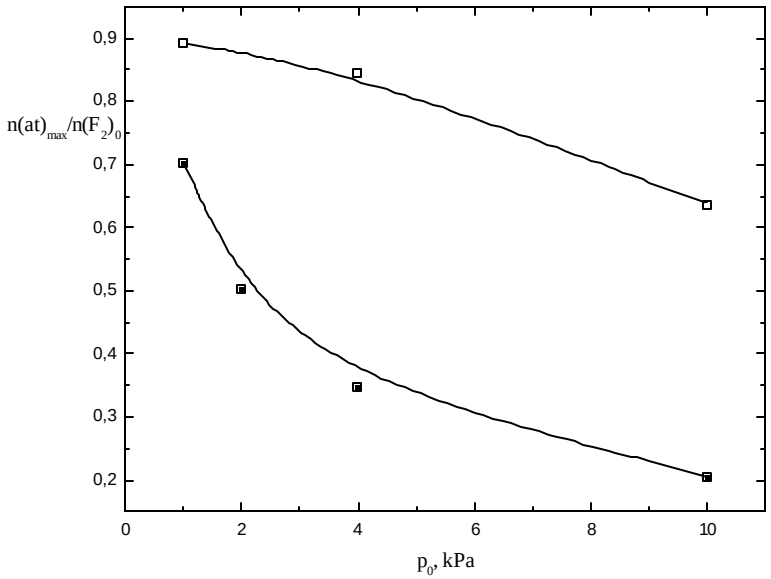

Fig. 41. Conversion of F_2 to F atoms in mixture F_2+NO (solid), and conversion of F_2 to I atoms in mixture F_2+NO+HI(open) in dependence on initial pressure. Dilution [F_2]:[He] = 1:30.

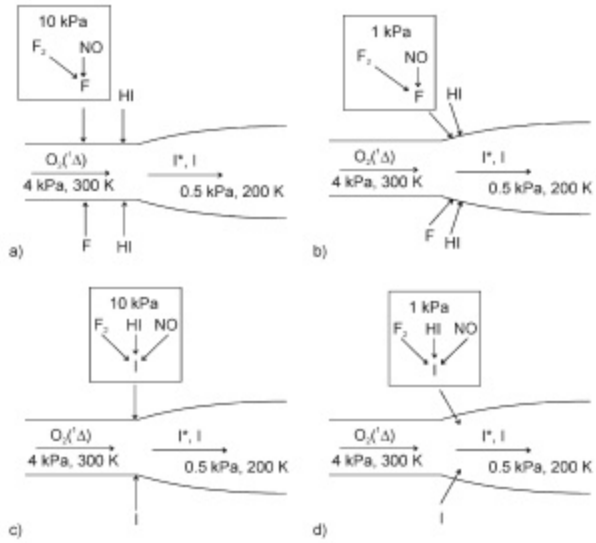

Fig. 42. Mixing schemes for I^* production: a) subsonic mixing of F, HI and $O_2(^1\Delta_g)$, a) supersonic mixing of F, HI and $O_2(^1\Delta_g)$, c) subsonic mixing of I and $O_2(^1\Delta_g)$, d) supersonic mixing of I and $O_2(^1\Delta_g)$.

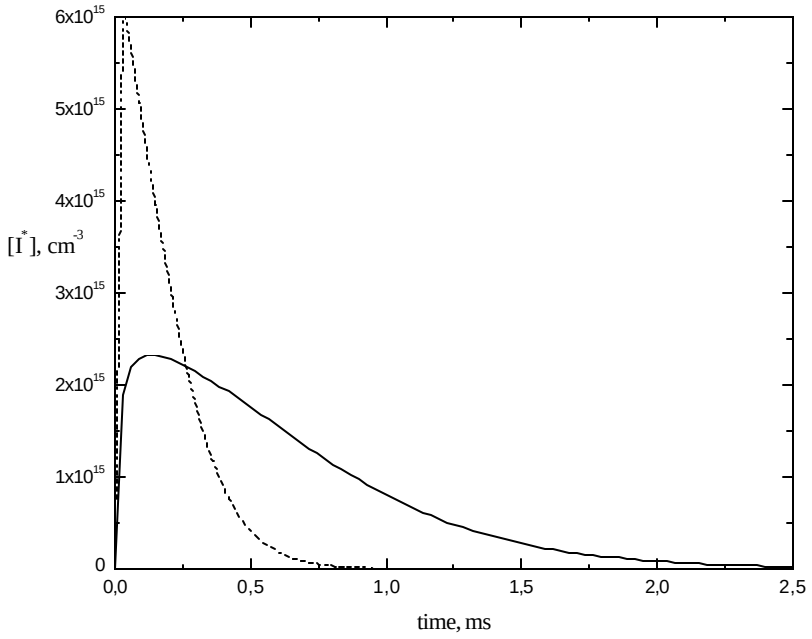

Fig. 43. Concentration profiles of I^* atoms for subsonic conditions. Mixing of F, HI and $O_2(^1\Delta_g)$ (—), and mixing of I and $O_2(^1\Delta_g)$ (…)

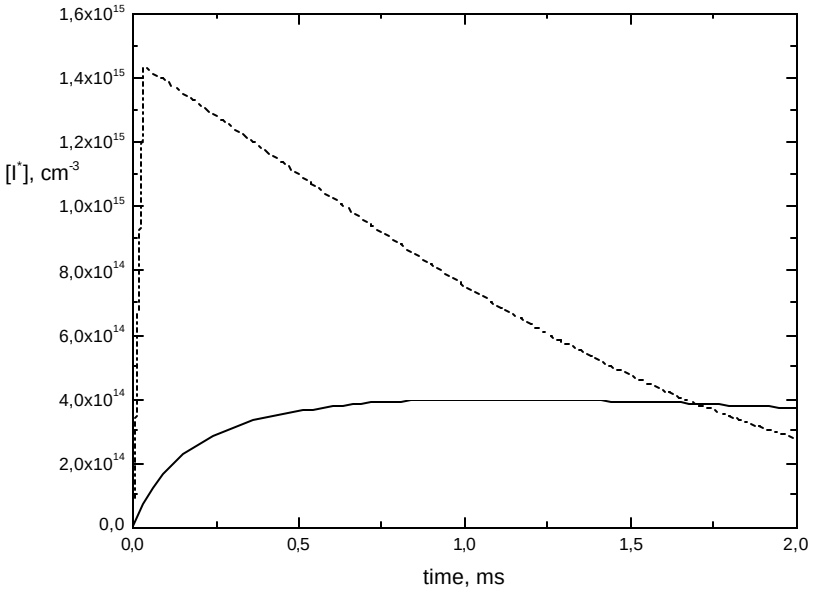

Fig. 44. Concentration profiles of I^* atoms for supersonic conditions. Mixing of F, HI and $O_2(^1\Delta_g)$ (—), and mixing of I and $O_2(^1\Delta_g)$ (…)

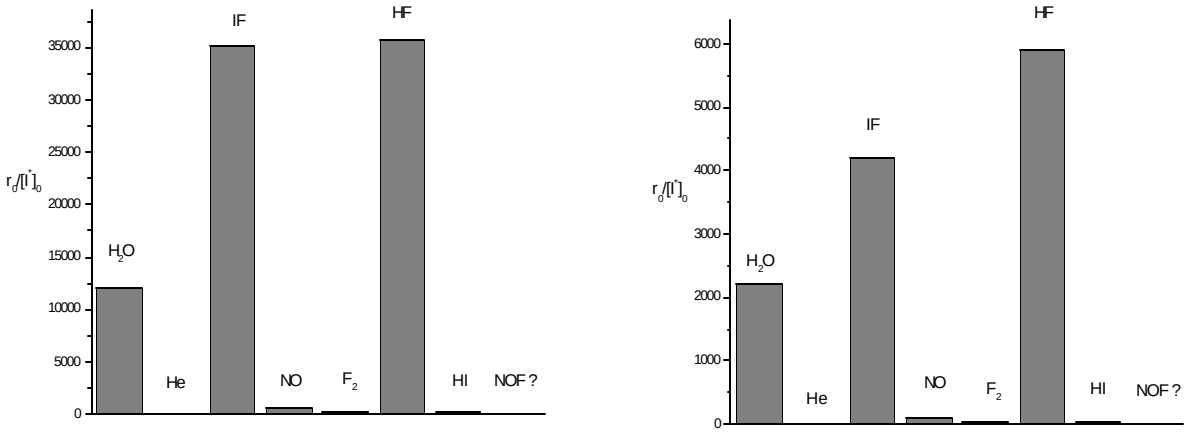

a) b)

Fig. 45 a, b. I* quenching by different molecules. a) subsonic mixing of I and $O_2(^1\Delta_g)$, b) supersonic mixing of I and $O_2(^1\Delta_g)$

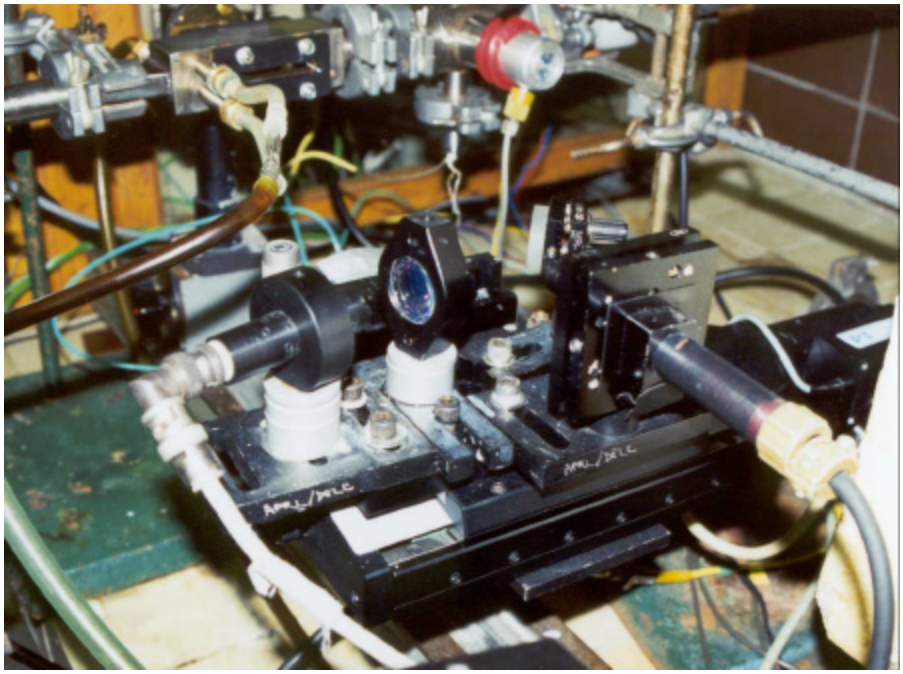

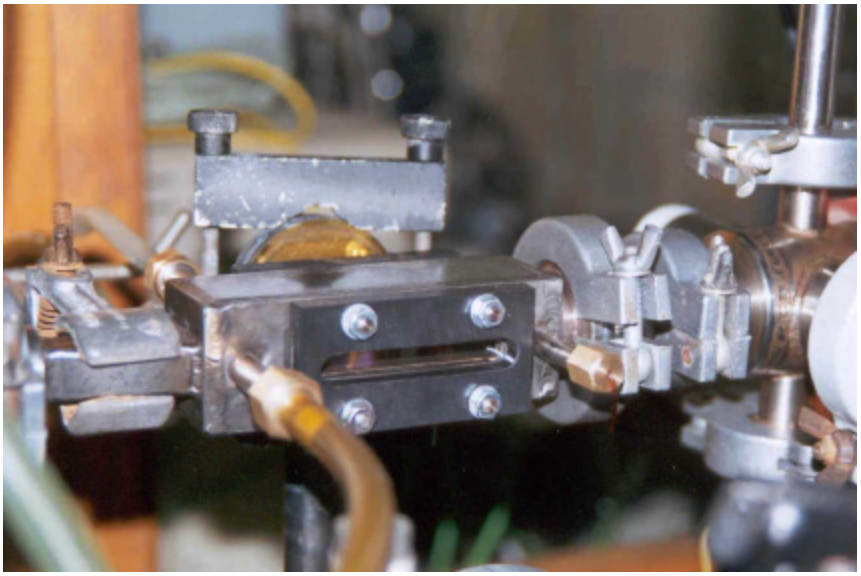

Photo 1 a, b